ACS APPLIED MATERIALS & INTERFACES

Research Article

www.acsami.org

ROP and ATRP Fabricated Dual Targeted Redox Sensitive Polymersomes Based on pPEGMA-PCL-ss-PCL-pPEGMA Triblock Copolymers for Breast Cancer Therapeutics

Arun Kumar,[†,§] Shantanu V. Lale,[†,§] Shveta Mahajan,[†,§] Veena Choudhary,[‡] and Veena Koul*[,†,§]

[†]Centre for Biomedical Engineering, and [‡]Centre for Polymer Science and Engineering, Indian Institute of Technology Delhi, New Delhi 110016, India

[§]Biomedical Engineering Unit, All India Institute of Medical Sciences, AIIMS, New Delhi 110029, India

Supporting Information

ABSTRACT: To minimize cardiotoxicity and to increase the bioavailability of doxorubicin, polymersomes based on redox sensitive amphiphilic triblock copolymer poly(polyethylene glycol methacrylate)-poly(caprolactone)-s-s-poly(caprolactone)-poly-(polyethylene glycol methacrylate) (pPEGMA-PCL-ss-PCL-pPEG-MA) with disulfide linkage were designed and developed. The polymers were synthesized by ring opening polymerization (ROP) of ε-caprolactone followed by atom transfer radical polymerization (ATRP) of PEGMA. The triblock copolymers demonstrated various types of nanoparticle morphologies by varying hydrophobic/hydrophilic content of polymer blocks, with PEGMA content of ~18% in the triblock copolymer leading to the formation of polymersomes in the size range ~150 nm. High doxorubicin loading content of ~21% was achieved in the polymersomes. Disulfide linkages were incorporated in the polymeric backbone to facilitate degradation of the nanoparticles by the intracellular tripeptide glutathione (GSH), leading to intracellular drug release. Release studies showed ~59% drug release in pH 5.5 in the presence of 10 mM GSH, whereas only ~19% was released in pH 7.4. In cellular uptake studies, dual targeted polymersomes showed ~22-fold increase in cellular uptake efficiency in breast cancer cell lines (BT474 and MCF-7) as compared to nontargeted polymersomes with higher apoptosis rates. *In vivo* studies on Ehrlich's ascites tumor (EAT) bearing Swiss albino mouse model showed ~85% tumor regression as compared to free doxorubicin (~42%) without any significant cardiotoxicity associated with doxorubicin. The results indicate enhanced antitumor efficacy of the redox sensitive biocompatible nanosystem and shows promise as a potential drug nanocarrier in cancer therapeutics.

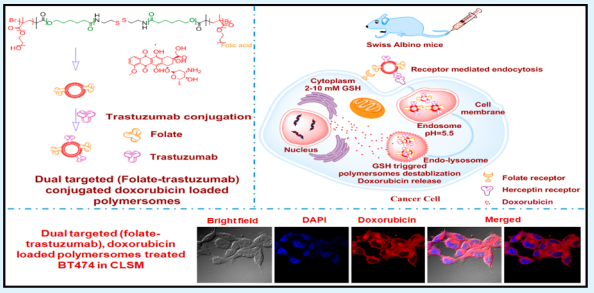

KEYWORDS: *cellular uptake, Ehrlich's ascites tumor, folate, redox sensitive polymersomes, trastuzumab*

1. INTRODUCTION

Doxorubicin is a potent drug in cancer chemotherapy which suffers from side effects such as nonspecificity leading to cardiotoxicity and multidrug resistance. To overcome these side effects, various types of polymeric nanoparticles such as micelles, nanospheres, nanocapsules, and polymersomes are being studied for drug delivery.[1,2] Polymeric nanosystems are of great interest because of their ease of synthesis, scalability, and functionalization with specific ligands for active targeting. Amphiphilic block copolymers form a variety of self-assembled nanostructures which are categorized into micelles, worm-like micelles, and polymersomes.[3−5] These nanosystems have received tremendous attention in last two decades for drug delivery applications due to increased drug bioavailability, prolonged circulation time, and passive/active targeting ability.[4,5] Self-assembly offers the potential to manipulate the size and morphologies of nanoparticles by varying the molecular weight, surface functionalization, and hydrophobic/hydrophilic ratio in the block copolymer.[6,7] Polymersomes are self-assembled bilayer vesicular entities in which a large aqueous core is enclosed in a polymeric wall of 10−15 nm thickness.[8] Structurally, they are robust in nature and can encapsulate both hydrophilic and hydrophobic molecules.[9,10]

Block copolymeric systems can be synthesized by different polymerization techniques such as ring opening polymerization (ROP),[11,12] reversible-addition−fragmentation transfer polymerization (RAFT),[13,14] atom transfer radical polymerization (ATRP),[15−17] and nitroxide mediated polymerization (NMP).[18] ROP is the most efficient method for the synthesis of polyesters. Cyclic esters (lactones) are polymerized by ROP using tin(II) octoate as catalyst and amine or alcohol as initiator.[11] ATRP is a living radical polymerization technique widely used for the synthesis of well-defined controlled molecular weight polymers with low polydispersity indices.[15−17] The mechanism of ATRP involves reversible deactivation of propagating radicals by a transition metal

Received: February 25, 2015
Accepted: April 2, 2015
Published: April 2, 2015

DOI: 10.1021/acsami.5b01731
ACS Appl. Mater. Interfaces 2015, 7, 9211−9227

Scheme 1. Schematic Illustration of Dual Targeted (Folic Acid and Trastuzumab) Redox Sensitive pPEGMA-PCL-ss-PCL-pPEGMA Polymersomes for Cancer Targeting

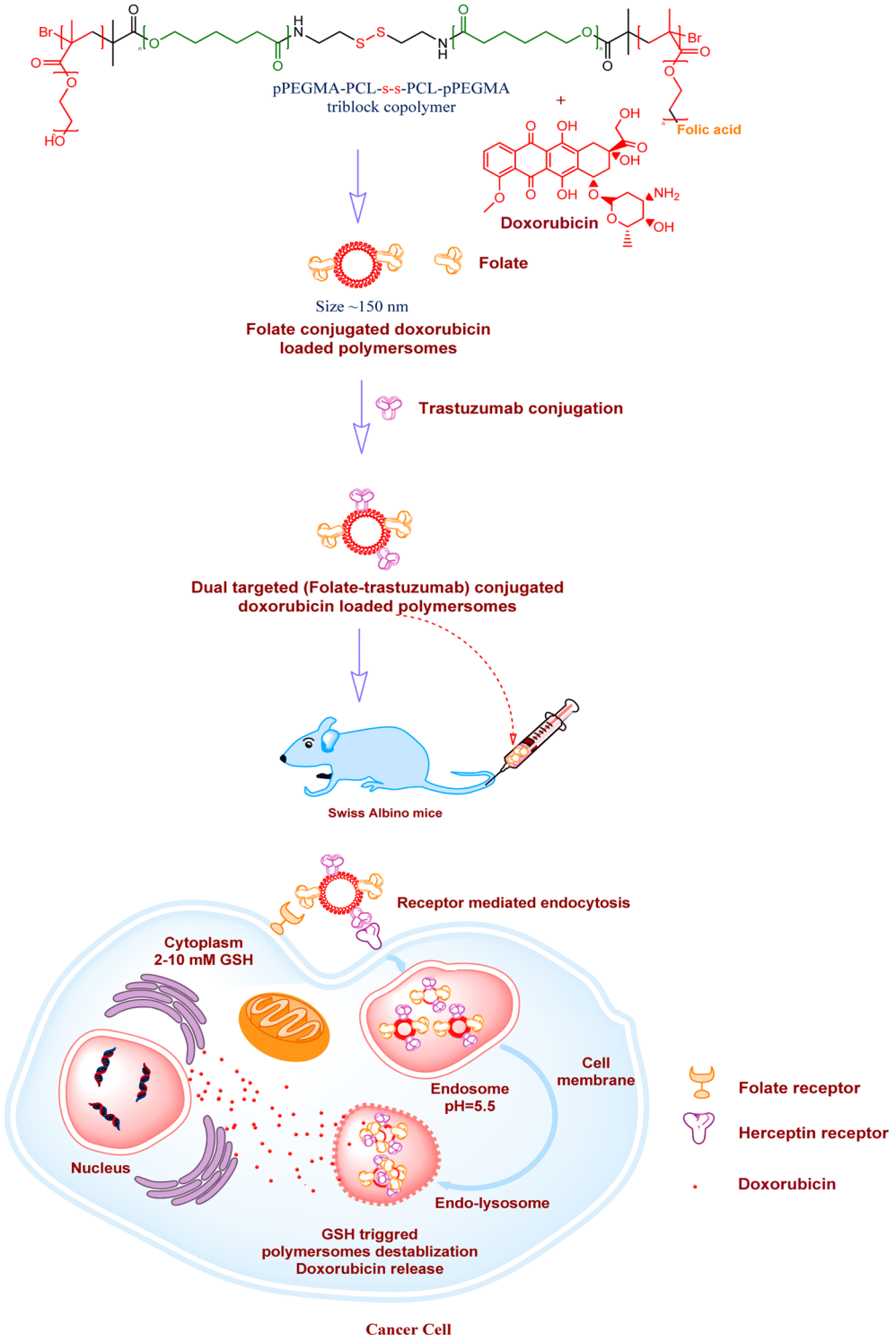

complex. The rate of initiation is much faster than the rate of propagation leading to controlled chain growth.

Polymers can be tailor-made to selectively release the therapeutic payload by triggering mechanisms such as pH, temperature, light, or redox sensitivity.[19−21] Change in redox potential is a promising mechanism for intracellular drug delivery.[22] In recent years, polymers with disulfide linkages have generated great interest because they exhibit stability in systemic circulation but degrade in the intracellular environment in the presence of glutathione (GSH).[23−25] Glutathione is a thiol containing tripeptide found in sufficient amounts in cell cytoplasm (1−10 mM) but in much lower concentrations in the blood plasma (2−20 μM).[26] In tumor cells, cytosolic GSH is found in concentrations several times higher than that in normal cells.[26−28] Thus, the nanoparticles designed with incorporation of disulfide linkages hold promise for intracellular

DOI: 10.1021/acsami.5b01731
ACS Appl. Mater. Interfaces 2015, 7, 9211−9227

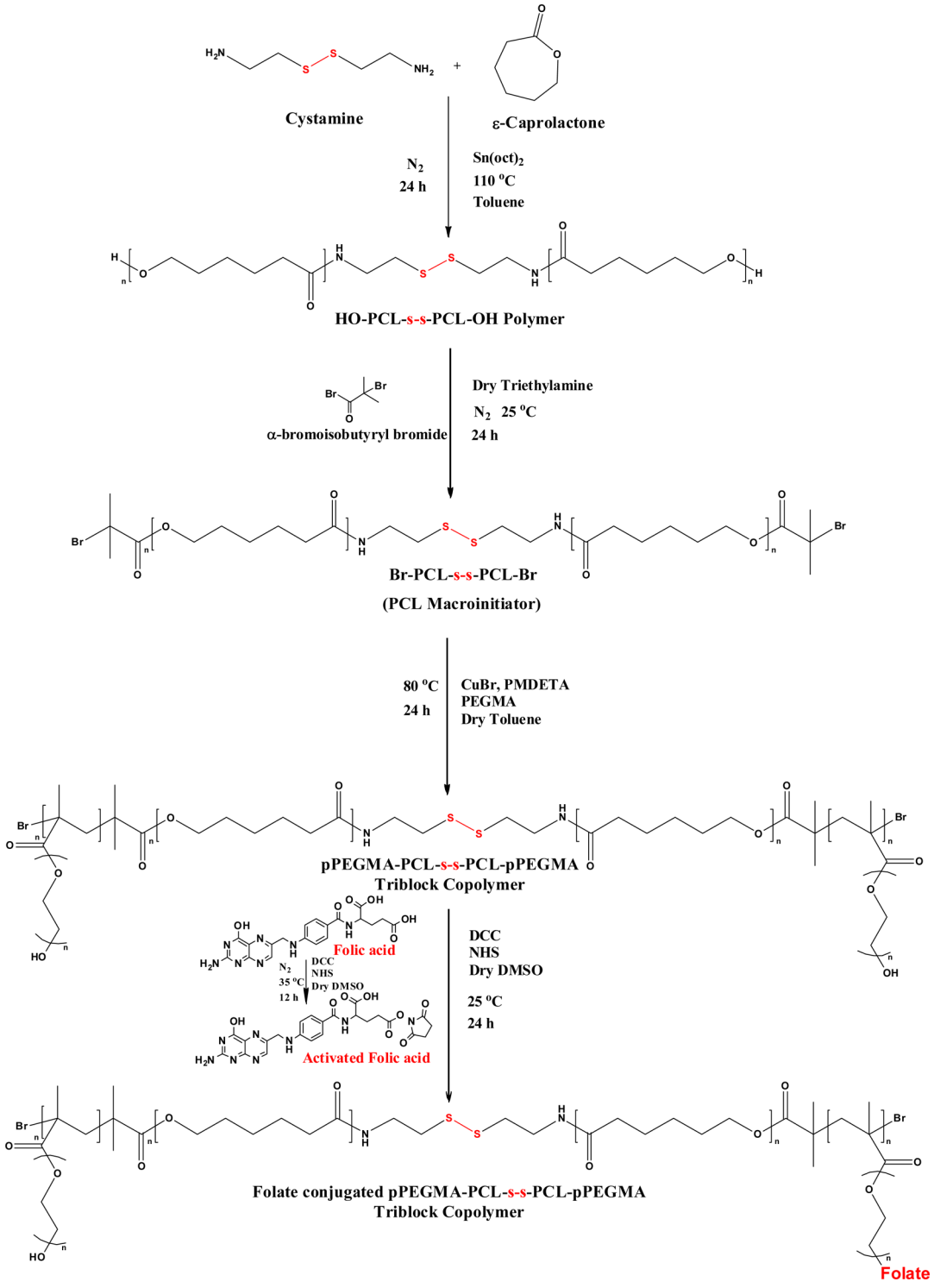

Figure 1. Schematic representation of triblock copolymer synthesis by ROP and ATRP.

delivery of chemotherapeutic drugs. To decrease opsonization and thereby increase *in vivo* circulation time, these nanosystems are often PEGylated. The PEG shell creates a water bound layer which does not allow proteins to adhere to the nanosystems.[29−31]

Active targeted therapy can be achieved by ligand conjugation to polymeric nanocarriers to increase the specificity of nanoparticles. Various types of ligands such as folic acid, antibodies, hormones, sugars, etc. have been studied for cancer targeting.[32] Folic acid has been widely used for functionalization of nanoparticles because the folic acid requirement increases in rapidly growing cancer cells. Trastuzumab (Herceptin) is a monoclonal antibody which targets the human epidermal growth factor receptor (HER2) and is widely used for targeting HER2 overexpressing cells in breast cancer.[33]

Targeting of cancer cells using two or multiple ligands conjugated to nanoparticles is a recent trend and is hypothesized to be a highly effective approach in cancer therapy.[34] Cancer cells generally overexpress many receptors on their surfaces, and hence, it is widely reported that dual or

DOI: 10.1021/acsami.5b01731
ACS Appl. Mater. Interfaces 2015, 7, 9211−9227

multiple targeted nanosystems result in higher uptake as compared to that of single targeted nanosystems.[34−36]

The aim of this study was to develop dual functionalized (folic acid and trastuzumab conjugated) redox sensitive polymersomes based on pPEGMA-PCL-ss-PCL-pPEGMA polymers and to study degradation, drug loading, and release behavior, *in vitro* and *in vivo* evaluation of its biocompatibility, and therapeutic efficacy (Scheme 1). Polymerization was carried out by ring opening polymerization to incorporate disulfide linkage in the polymer backbone. ATRP was used for controlled polymerization of poly(ethylene glycol) methacrylate (PEGMA) using a polycaprolactone macroinitiator. Multiple pendant chains of polyethylene glycol impart hydrophilicity which avoids macrophage recognition and enhance circulation life of polymeric nanoparticles. The copolymers were further explored for polymersome formation. *In vitro* biological studies including biocompatibility assays such as MTT, hemolytic study, coagulation studies, and protein adsorption study were also performed. Doxorubicin was encapsulated in the polymersomes, and release studies were carried out at pH 7.4 and pH 5.5 in the presence and absence of 10 mM GSH. Cellular uptake and apoptosis studies of doxorubicin loaded polymersomes were carried out using confocal laser scanning microscopy (CLSM) and fluorescence activated cell sorting (FACS). *In vivo* studies were carried out to evaluate tumor reduction efficacy of dual targeted doxorubicin loaded polymersomes.

2. MATERIALS AND METHODS

2.1. Materials. ε-Caprolactone, cystamine dihydrochloride (Cys.2HCl), poly(ethylene glycol) methacrylate (PEGMA, M_n = 360), tin(II) 2-ethylhexanoate ($Sn(oct)_2$), copper(I) bromide (CuBr), α-bromoisobutyryl bromide (α-BriBr), *N*,*N*,*N*′,*N*′,*N*″-pentamethyldiethylenetriamine (PMDETA), *N*,*N*′-dicyclohexylcarbodiimide (DCC), *N*-hydroxylsuccinimide (NHS), fluorescein isothiocyanate (FITC), dithiothreitol (DTT), glutathione reduced (GSH), propidium iodide (PI), and phosphotungstic acid (PTA) for microscopy, 3-(4,5-dimethyl-2-thiazolyl)-2,5-diphenyl-tetrazolium bromide (MTT), and bovine serum albumin (BSA) were purchased from Sigma-Aldrich (St. Louis, MO, USA). Cys·2HCl was used after the removal of hydrochloric acid by washing with 5% (w/v) sodium hydroxide. PEGMA was used after the removal of inhibitor (MEHQ) by passing through a basic alumina column and drying over activated 3 Å molecular sieves. CuBr was purified by washing with acetic acid, ethanol, and diethyl ether before use. Anhydrous sodium sulfate (Na_2SO_4), sodium bicarbonate ($NaHCO_3$), sodium acetate, acetic acid, and Triton X-100 were obtained from Merck Millipore, Mumbai, India and used as received. Toluene, dichloromethane (DCM), diethyl ether, tetrahydrofuran (THF), and methanol were purchased from Merck Millipore, India. Toluene was dried by distillation over a sodium-benzophenone mixture before use. Dialysis membranes (3.5 kDa) were purchased from Himedia, Mumbai, India. Penicillin−streptomycin solution, fetal bovine serum (FBS), Dulbecco's modified Eagle's medium (DMEM), and RPMI were obtained from Gibco Life Technologies (NY, USA). Herclon (trastuzumab for injection) (Roche, India) was purchased and purified by dialysis in PBS before use. Doxorubicin gift sample was obtained from Ranbaxy Laboratories Ltd., New Delhi. MCF-7, L929, and BT474 cells were obtained from NCCS, Pune. An Annexin V-FITC assay kit was obtained from BD Biosciences (San Jose, USA). Ultrapure water (18.2 MΩ-cm resistivity) was used for all of the experiments.

2.2. Synthesis of Triblock Copolymers (pPEGMA-PCL-ss-PCL-pPEGMA). Triblock copolymers were synthesized in three steps as shown in Figure 1. In the first step, polycaprolactone diol with a disulfide core was synthesized by ring opening polymerization of ε-caprolactone. In the second step, polycaprolactone diol was converted to the polycaprolactone macroinitiator. In the third step, pPEGMA-PCL-ss-PCL-pPEGMA polymers were synthesized using ATRP with varying ratios of PEGMA to macroinitiator (1:6−1:24).

2.2.1. Synthesis of Polycaprolactone Diol (HO-PCL-ss-PCL-OH). HO-PCL-ss-PCL-OH was synthesized by ring opening polymerization of ε-caprolactone using cystamine as initiator and tin(II) 2-ethylhexanoate as catalyst. Cystamine (100 mg, 0.66 mmol), ε-caprolactone (initiator/monomer ratio 1:132, 9.89 g, 86 mmol) were dissolved in dry toluene (10 mL) in the Schlenk tube followed by the addition of tin(II) 2-ethyl hexanoate (5 mol % of initiator, 10.63 μL, 0.0328 mmol), and polymerization was carried out at 110 °C for 24 h under N_2 atmosphere. After the completion of the reaction, toluene was removed under vacuum in a rotary evaporator. The viscous crude product was isolated by precipitating three times in cold diethyl ether and was characterized with ^{1}H NMR (Brukers, USA) and gel permeation chromatography (GPC) (Waters, USA). Yield = 86%. GPC analysis was performed on a Waters liquid chromatography system fitted with a refractive index detector (Waters 2414) and Styragel HR 3 and HR 4 columns. The measurements were performed using THF as mobile phase at a flow rate of 1.0 mL/min at 30 °C, and a series of polystyrene standards were used for molecular weight calibration.

^{1}H NMR (300 MHz, $CDCl_3$, δ (ppm)) −1.38 (m, -OCH_2CH_2-***CH_2***CH_2CH_2CO-), 1.62 (m, -OCH_2***CH_2***CH_2***CH_2***CH_2CO-), 2.28 (t, -$OCH_2CH_2CH_2CH_2$***CH_2***CO-), 2.8 (t, -$NHCH_2$***CH_2***-SS-***CH_2***CH_2NH-), 3.55 (t, -NH***CH_2***CH_2-SS-CH_2***CH_2***NH-, (cystamine core)), 3.6 (t, -***CH_2***OH) (terminal OH groups), 4.06 (t, -O***CH_2***CH_2CH_2-CH_2CH_2CO-), M_n (GPC) = 20 400 Da; molecular weight distribution (MWD), 1.50; M_n (NMR) = 12 890 Da.

2.2.2. Synthesis of the Bromine-Terminal PCL-ss-PCL Macroinitiator. HO-PCL-ss-PCL-OH ($M_{n\ (NMR)}$ = 12 890 Da, 0.5 g, 0.0388 mmol) was dissolved in dry DCM in a Schlenk tube, followed by the addition of dry triethylamine (19.62 mg, 0.194 mmol). α-BriBr (44.42 mg, 0.194 mmol) was added to the Schlenk tube at 0 °C, and the reaction was allowed to continue with continuous stirring for 24 h at 25 °C under N_2 atmosphere. Progress of the reaction was followed by ^{1}H NMR. At the end of the reaction, the reaction mixture was filtered and concentrated, and the resulting viscous solution was dissolved in 100 mL of DCM and extracted with a saturated solution of $NaHCO_3$ to remove unreacted α-BriBr. After extraction, the organic layer was recovered and dried over anhydrous Na_2SO_4 and evaporated under vacuum. The viscous crude solution was purified by precipitation in cold diethyl ether twice and was characterized with ^{1}H NMR (Brukers, USA). Yield = 90%

^{1}H NMR (300 MHz, $CDCl_3$, δ (ppm) −1.36 (m, -OCH_2CH_2***CH_2***CH_2CH_2CO-), 1.64 (m, -OCH_2***CH_2***CH_2***CH_2***CH_2), 1.96 (s, -CH_2OCO C(***CH_3***)$_2$Br), 2.32 (t, -$OCH_2CH_2CH_2CH_2$-***CH_2***CO−), 3.65 (t, -NH-***CH_2***CH_2-SS-CH_2***CH_2***-NH-,(cystamine core)), 2.75 (t, -$NHCH_2$***CH_2***-SS-***CH_2***CH_2NH-), 4.07 (t, -O***CH_2***$CH_2CH_2CH_2CH_2CO$-), 4.18 (t, -***CH_2***$OCOC(CH_3)_2$Br (terminal group)).

2.2.3. Synthesis of pPEGMA-PCL-ss-PCL-pPEGMA Triblock Copolymers. Copper(I) bromide (CuBr) (44 mg; 2 mmol) and PMDETA (64 μL; 2 mmol) were added to dry toluene (5 mL) in a Schlenk tube under N_2 atmosphere. When a blue complex was formed, PEGMA (M_n = 360 Da, 300 μL; 6 mmol) and the PCL macroinitiator (2.0 g; 1 mmol) were added, and the reaction mixture was allowed to stir at 90 °C for 24 h under nitrogen atmosphere. Macroinitiator, CuBr, and PMDETA were taken in the ratio of 1:2:2, while the PEGMA to macroinitiator ratio was varied from 6 to 24 mmol for obtaining different molecular weight polymers. After completion of the reaction, the product was purified by passing through a basic alumina column using dichloromethane. The elute was concentrated over a rotary evaporator, and the viscous crude solution was precipitated in cold diethyl ether twice. The polymer was obtained as a white solid and was characterized by ^{1}H NMR (Brukers, USA) and GPC (Waters, USA). The polymer designations, compositions, and yields are given in Table 1. Four polymers were reported (P6, P9, P12, and P24) in which the ratio of PEGMA to PCL was increased from P6 to P24 with increase in hydrophilicity.

DOI: 10.1021/acsami.5b01731
ACS Appl. Mater. Interfaces 2015, 7, 9211−9227

Table 1. Polymer Designations and Compositions

polymer notations	initiator/ monomer ratio	macroinitiator (PCL-Br) (mmol)	monomer (PEGMA) (mmol)	yield (%)
P6	1:6	0.155	0.930	72
P9	1:9	0.155	1.396	76
P12	1:12	0.155	1.862	70
P24	1:24	0.155	3.724	74

^{1}H NMR (300 MHz, $CDCl_3$, δ (ppm) −1.40 (m, -$OCH_2CH_2\boldsymbol{CH_2}CH_2CH_2CO$−), 1.62 (m, -$OCH_2\boldsymbol{CH_2}$-$CH_2\boldsymbol{CH_2}CH_2CO$-), 2.40−2.25 (t, $OCH_2CH_2CH_2\boldsymbol{CH_2}CO$-), 2.8 (t, -$NHCH_2\boldsymbol{CH_2}$-SS-$\boldsymbol{CH_2}CH_2NH$-), 3.6 (t, -NH-$\boldsymbol{CH_2}CH_2$-SS-$CH_2\boldsymbol{CH_2}$-NH-), 3.5−3.7 (m, -$O\boldsymbol{CH_2CH_2}O$-) (PEG), 4.08 (t, -$O\boldsymbol{CH_2}CH_2CH_2CH_2CH_2CO$-), 4.3 (t, -$\boldsymbol{CH_2}OCOC(CH_3)_2$-PEGMA).

Polymer notations are given on the basis of monomer to initiator ratio (e.g., P6 means the PEGMA to macroinitiator ratio is six and so on).

2.3. DTT Triggered Degradation of pPEGMA-PCL-ss-PCL-pPEGMA. To check the redox sensitive behavior of triblock copolymers, degradation of triblock copolymers was carried out in the presence of 10 mM DTT. Polymeric samples (50 mg) were dissolved in DMSO (2 mL) containing DTT (10 mM, 3.8 mg) and stirred at 37 °C for 24 h. The degradation products were purified by precipitation from cold diethyl ether and analyzed by GPC and ^{1}H NMR.

2.4. Conjugation of Folic Acid to pPEGMA-PCL-ss-PCL-pPEGMA Triblock Copolymers. Folic acid (68.5 mg, 0.155 mmol) was dissolved in dimethyl sulfoxide (10 mL). DCC (64 mg, 0.310 mmol) and NHS (35.7 mg, 0.310 mmol) were added to the reaction mixture, and the reaction was allowed to stir for 12 h under nitrogen atmosphere. Triblock copolymer pPEGMA-PCL-ss-PCL-pPEGMA (2 g, 0.155 mmol) was further added to the reaction mixture, and the reaction was allowed to stir for another 12 h under inert atmosphere. After the completion of the reaction, the excess amounts of activated folic acid, DCC, and NHS were removed by dialysis followed by lyophilization. The obtained polymer was characterized by FTIR.

2.5. Preparation and Characterization of Nanoparticles. Nanoparticles were prepared by nanoprecipitation method.[37−39] Ten milligrams of the folate conjugated pPEGMA-PCL-ss-PCL-pPEGMA triblock copolymers (P6−P24) was dissolved in 1 mL of THF and added dropwise to 10 mL of water with continuous stirring. The dispersions were allowed to stir for 12 h to evaporate the organic solvent. The nanoparticle suspension was washed three times with water at 4000 rpm for 15 min using an Amicon ultracentrifuge filter (30 kDa). Purified nanoparticles were further suspended in water for size and morphological analysis.

To establish the core−shell morphology of polymeric nanoparticles, fluorescein isothiocyanate (FITC) and propidium iodide (PI) were loaded in the polymer nanoparticles. Dye loaded nanoparticles were prepared by the solvent evaporation method. The copolymer P12 (10 mg/mL) was dissolved in $CHCl_3$ and mixed with FITC and PI (1 mg/mL) solution in water, and the mixture was homogenized at 10,000 rpm for 1 min. The solution was added dropwise to water with continuous stirring and kept stirring overnight to remove the residual solvent. The morphology of dual dye loaded nanoparticles was characterized by confocal laser scanning microscopy (FluoView FV1000, Olympus, USA).

The size and zeta potential of polymeric nanoparticles were measured on a DLS Zetasizer Nano ZS instrument (Malvern Instruments Ltd., UK) with 173° optics at a temperature of 25 °C. Measurements were performed in triplicate with 0.1 mg/mL concentration of nanoparticle dispersion. SEM, TEM, and confocal microscopy were carried out to analyze particle morphology. SEM images were acquired with a ZEISS EVO 50, (Carl Zeiss Microscopy, GmbH, Germany) with 2.0 nm resolution at an acceleration voltage of 0.2 to 30 kV. TEM images were acquired using a Jeol 2100F (Jeol, USA) field emission microscope with 200 kV accelerating voltage. Samples were prepared by dipping a carbon-coated copper grid in nanoparticle dispersion for 1 min and then in 1% PTA (for negative staining) for 30 s followed by drying at 35 °C. Atomic force microscopy (AFM) (Nanoscope III Digital Instrument 5.31R1, Digital Instruments, Inc. USA) was used for surface morphological characterization of colloidal polymer nanoparticles.

2.6. Colloidal Stability. Colloidal stability of nanoparticles was studied using the turbidimetry method where nanoparticles were suspended in various media including water, phosphate buffered saline (PBS) at pH 7.4, cell culture medium (RPMI supplemented with 10% FBS), and NaCl (1 M). Nanoparticle dispersions (1.0 mg/mL) were prepared in the different media, and optical density was measured as a function of time using UV−visible spectrophotometry (BioTek PowerWave XS2) at 500 nm. Stability of P12 nanoparticles was studied in aqueous medium at pH 7.4 with and without 10 mM GSH using DLS for 24 h.

2.7. Protein Adsorption Study. Weighed amounts (5 mg) of polymer nanoparticles were incubated with 10 mL of 4% BSA solution in PBS at 37 °C for 24 h at 100 rpm. After 24 h, the solution was centrifuged at 26,200 rpm for 30 min, and protein content in the supernatant was quantified. The supernatant (1 mL) was incubated with Biuret reagent (4 mL) at 37 °C for 20 min at 100 rpm. To determine the concentration of unadsorbed protein in the supernatant, a UV−visible spectrophotometer was used at 540 nm. A calibration curve was prepared from known concentrations of BSA solutions (500−2500 μg/mL), subjected to the same treatment.[40,41]

2.8. Blood Compatibility. Nanoparticle blood compatibility was determined using hemolysis and coagulation studies. Blood samples were obtained from the blood bank at AIIMS, New Delhi.

2.8.1. Hemolysis Study. Hemolysis study was carried out to evaluate the biocompatibility of the polymeric nanoparticles with red blood cells (RBCs). RBCs were separated by centrifugation at 1500 rpm for 5 min. RBCs were then washed three times with PBS, and 50 μL of RBCs was diluted with 10 mL of PBS to form the stock solution. Polymer nanoparticle concentrations were prepared in PBS in the range of 1 to 4 mg/mL. One hundred microliters of each concentration was incubated with 100 μL of RBC stock solution at 37 °C for 30 min at 120 rpm to get final concentrations in the range 0.5−2 mg/mL. The mixture was then centrifuged at 1500 rpm for 5 min. The supernatant was analyzed using a UV−visible spectrophotometer at 540 nm. Hemolysis was quantified based on the positive control (1% Triton X 100) and negative control (PBS) as per eq 1.

$$\%\ \text{Hemolysis} = \frac{A_{\text{Sample}} - A_{\text{Negative}}}{A_{\text{Positive}} - A_{\text{Negative}}} \times 100 \quad (1)$$

where A_{Sample} is the absorbance of the supernatant of nanoparticles dispersion. A_{Negative} is the absorbance of the supernatant of PBS, while A_{Positive} is the absorbance of the supernatant of RBCs treated with 1% Triton X 100.

2.8.2. Coagulation Studies. Nanoparticles were incubated with 1 mL of plasma in varying concentrations (100−500 μg/mL) for 1 h at 37 °C. For the measurement of PT, excess $CaCl_2$ solution was added to the plasma to initiate clotting. For the measurement of aPTT, the plasma was incubated with kaolin reagent (5 mg/mL) for 3 min to initiate the intrinsic pathway of coagulation followed by the addition of $CaCl_2$ solution. Measurement of time taken for fibrin clot formation was determined using an automated coagulation analyzer (Diagnostica Stago, Germany).

2.9. Drug Loading and Release. Doxorubicin was loaded in the polymersomes according to the method reported by Sanson et al.[42] On the basis of nanoparticle size, morphology, and stability, the P12 polymer formed stable polymersomes, and hence,the drug loading studies were carried out with the P12 polymer. Twenty-five milligrams of doxorubicin hydrochloride and 50 mg of folate conjugated polymer (P12) were dissolved in 5 mL of DMSO with sonication for 60 s. The solution was then added to 50 mL of bicarbonate buffer (pH 10.5) with continuous stirring. The drug loaded polymersomes were dialyzed against phosphate buffer (pH 7.4) for 6 h.

DOI: 10.1021/acsami.5b01731
ACS Appl. Mater. Interfaces 2015, 7, 9211−9227

Drug loading content and encapsulation efficiency were calculated by measuring absorbance of doxorubicin at 481 nm using a UV−visible spectrophotometer (PerkinElmer Lambda 25, USA) as shown in eqs 2 and 3.

$$\text{Drug loading content \%)} = \frac{\text{weight of drug loaded in nanoparticles}}{\text{weight of nanoparticles}} \times 100 \quad (2)$$

$$\text{Drug encapsulation efficiency (\%)} = \frac{\text{amount of drug loaded in nanoparticles}}{\text{total drug taken}} \times 100 \quad (3)$$

For drug release, 10 mL of drug loaded nanoparticles (0.9 mg/mL polymer concentration) was taken in a dialysis membrane (MWCO 12−14 kDa) and suspended in release media with continuous stirring. Release media included PBS (pH 7.4) and sodium acetate buffer (pH 5.5) with and without 10 mM GSH. Release was studied up to 96 h. One milliliter aliquots were removed from the external medium at definite intervals and replaced with an equal volume to maintain sink conditions.

2.10. Preparation of Trastuzumab Conjugated Polymersomes. Trastuzumab conjugated polymersomes were prepared by EDC-NHS chemistry. Folate conjugated polymersomes were suspended in mili-Q water (DNase/RNase free) at a concentration of 1 mg/mL. EDC (100 μL, 200 mmol) and NHS (100 μL, 100 mmol) were added to the nanoparticle suspension at 25 °C with mild stirring for 30 min. Trastuzumab (200 μL, 3 mg/mL in PBS) was then added to the reaction medium for 30 min with mild stirring at 25 °C. The polymersomes were then dialyzed and washed with an Amicon ultracentrifuge filter. Finally, folate−trastuzumab conjugated polymersomes were characterized by zeta potential, energy dispersive X-ray analysis (EDX), and X-ray photoelectron spectroscopy (XPS). The above synthesis reaction procedure was followed with the native nonconjugated polymersomes to form trastuzumab conjugated polymersomes. Polymersome composition based on attached targeting moieties is shown in Table 2.

Table 2. Polymersome Composition (P12) Depending on Attached Targeting Moieties

polymersomes	composition
Tri-ss-NPs	native nonconjugated polymersomes
Tri-ss-Dox-NPs	native nonconjugated doxorubicin loaded polymersomes
Tri-ss-FA-Dox- NPs	folate conjugated doxorubicin loaded polymersomes
Tri-ss-Her-Dox-NPs	trastuzumab conjugated doxorubicin loaded polymersomes
Tri-ss-FA-Her-Dox-NPs	folate−trastuzumab conjugated doxorubicin loaded polymersomes

2. 11. Cell Line Studies. *2.11.1. MTT Cell Viability Assay.* The cytocompatibility of the polymeric nanoparticles was evaluated in MCF-7 (cancer cell line) using the MTT assay according to the protocol.[43] Cells were seeded in a 96-well plate at a density of 1×10^4 cells per well in DMEM medium supplemented with 10% FBS and 1% penicillin−streptomycin as antibiotic and incubated at 37 °C for 24 h in CO_2 atmosphere. Cells were incubated with nanoparticle dispersion in concentration ranging from 0.5 to 2.0 mg/mL. PBS and 1% Triton X 100 were used as negative and positive controls, respectively. After 24 h of incubation, the cells were incubated with 10 μL (5 mg/mL) of MTT for 4 h. The purple formazan crystals formed were dissolved in 200 μL of dimethyl sulfoxide, and absorbance was measured at 540 nm. Cell viability was calculated using eq 4.

$$\text{Cell viability (\%)} = \frac{A_{\text{Sample}} - A_{\text{Positive}}}{A_{\text{Negative}} - A_{\text{Positive}}} \times 100 \quad (4)$$

where A_{sample} is the absorbance of cells treated with nanoparticles, and A_{negative} and A_{positive} are the absorbance of cells treated with PBS and 1% Triton X 100, respectively.

2.11.2. In Vitro Cellular Uptake Studies Using Confocal Laser Scanning Microscopy. The cellular uptake of nanoparticles by BT474, MCF-7, and L929 cells were analyzed using confocal laser scanning microscopy. Cells were seeded at a density of 5×10^4 cells/well in a six well plate and incubated in a CO_2 incubator at 37 °C for 24 h. Cells were treated with polymersomes at concentrations equivalent to 10 μg of doxorubicin and incubated for 4 h at 37 °C in CO_2 incubator. After 4 h, cells were washed with PBS to remove excess nanoparticles, fixed with 4% paraformaldehyde solution, and stained with 20 μL of DAPI and were observed under CLSM at 100× magnification.

2.11.3. Cellular Uptake Studies Using Fluorescence Activated Cell Sorting (FACS)/Flow Cytometry. BT474, MCF-7, and L929 cells were seeded in six well plates at a density of 1×10^5 cells and incubated for 24 h in CO_2 incubator at 37 °C. Cells were treated with polymersomes with equivalent concentration of 10 μg of doxorubicin and incubated in a CO_2 incubator for 4 h at 37 °C. Cells were washed three times with PBS to remove excess polymersomes, trypsinized, and centrifuged at 3500 rpm for 5 min. Cells were suspended in 0.5 mL of PBS for cellular uptake analysis by flow cytometry (BD FACS Aria, BD Biosciences USA).

2.11.4. Annexin V-FITC Apoptosis Assay. To analyze cellular apoptosis and necrosis in BT474, MCF-7, and L929 cell line, 1×10^5 cells were seeded in six well plates and incubated for 24 h at 37 °C. Polymersomes with concentration equivalent to 10 μg of doxorubicin were incubated with cells for 7 h. Cells were washed three times with PBS and trypsinized and centrifuged at 3500 rpm for 5 min. Cells were then suspended with 0.5 mL of Annexin binding buffer and were incubated with 5 μL of Annexin V-FITC and 5 μL of propidium iodide solution in the dark for 10 min. The fluorescence of the cells was measured by flow cytometry, and apoptotic and necrotic cells were determined based on differential staining.

2.12. *In Vivo* Studies. Swiss albino mice (age 55−65 days) (weight 25 ± 5 g) were procured from a central animal facility, All India Institute of Medical Sciences (AIIMS), New Delhi, India (Ethical approval number 796/IAEC/14). The animal facility was environmentally controlled and maintained at 25 ± 1 °C and suitable relative humidity with 12 h light and dark cycle. Animals were fed chow food and purified water *ad libitum* throughout the study. Animals were randomized into three groups consisting of six mice per group for the study: the first group, doxorubicin (5 mg/kg); second group, Tri-ss-FA-Her-Dox-NPs (doxorubicin concentration equivalent to 5 mg/kg); and the third group, PBS as the control.

2.12.1. Tumor Induction and Evaluation of Antitumor Efficacy. Ehrlich's ascites tumor cell line (EAT) (murine breast carcinoma) was injected in mice for tumor induction. Mice were subcutaneously inoculated on the dorsal side with approximately 2×10^7 EAT cells and kept under observation for tumor onset. When the tumor volume reached around 200−250 mm^3, the day was designated as day zero, and treatment was started via tail vein with a volume of 150 μL at a 3 day time interval in the mice. Animal behaviors were monitored every day. Tumor volumes were measured with Vernier calipers, and tumor volume was calculated using eq 5.

$$V = 0.5 \times L \times W^2 \quad (5)$$

where V is the volume, L is the length, and W is the width of the tumor in millimeters. Mice were sacrificed on the 18th day after treatment. Blood and vital organs of mice were collected for serum biochemistry and histopathological analysis.

2.12.2. Histopathological Studies. To analyze the toxicity at the cellular level in different organs of mice, mice were sacrificed on the 18th day, and vital organs such as the heart, lung, liver, kidney, and spleen, along with the tumor, were removed for histological analysis. The tumor and organs were washed with PBS and stored in 4% formalin buffer solution. The slides were made by embedding the organ in paraffin, and then, sections were cut into 5 μm thick sections using a rotary microtome (Leica, USA), followed by staining with

DOI: 10.1021/acsami.5b01731
ACS Appl. Mater. Interfaces 2015, 7, 9211−9227

Table 3. Molecular Weights of Polymers Determined by GPC and ^{1}H NMR before and after DTT Degradation

		before degradation			after degradation		
polymer composition initiator/monomer	polymer notations	M_{nNMR}	M_{nGPC}	MWD_{GPC}[a]	M_{nNMR}	M_{nGPC}	MWD_{GPC}
1:6	P6	13285	25797	1.28	8980	10811	1.32
1:9	P9	14548	27427	1.25	7910	8389	1.76
1:12	P12	15718	28728	1.35	8160	8854	1.46
1:24	P24	21355	41283	1.25	10390	9588	1.15

[a]MWD: molecular weight distribution.

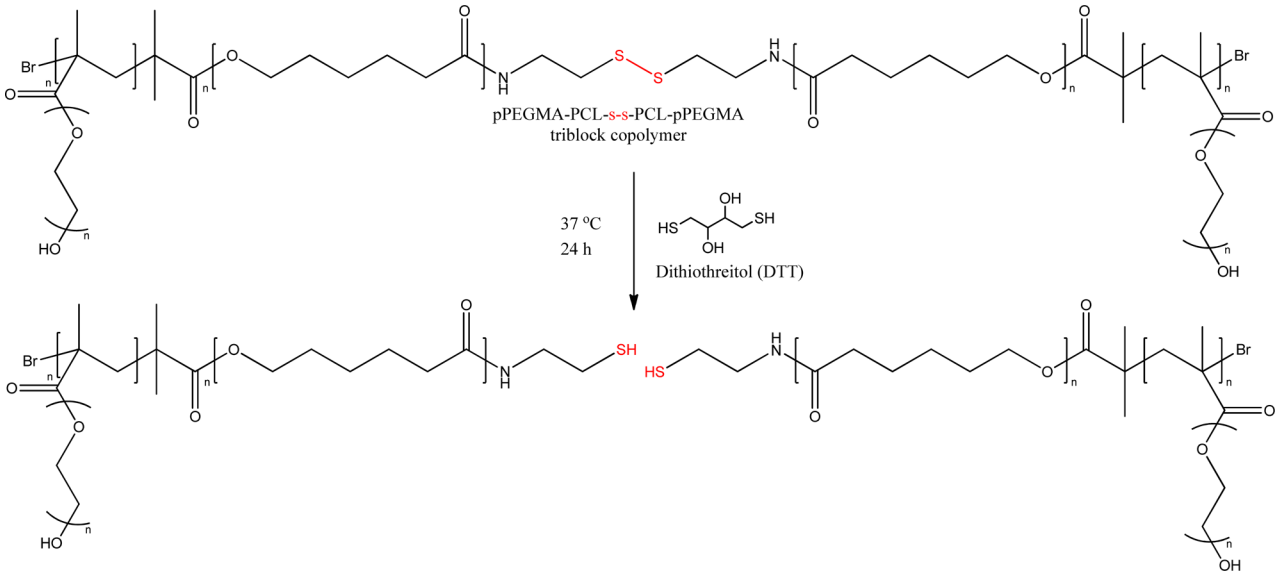

Figure 2. DTT triggered degradation of the triblock copolymer.

hematoxyline and eosin (H&E). Samples were analyzed to evaluate necrosis, inflammation, and damage of tissue.

2.12.3. Serum Biochemistry Analysis. Blood samples from tumor bearing mice were obtained to analyze the side effects of doxorubicin and dual targeted doxorubicin loaded polymersomes at the cellular level in treated mice.

For serum biochemistry, blood was allowed to clot and centrifuged at 3000 rpm for 10 min to obtain the serum. Serum samples were analyzed for blood parameters such as creatinine, uric acid, total protein, albumin, globulin, aspartate transaminase, alanine transaminase, alkaline phosphatase, cholesterol, and creatine kinase-MB (CK-MB) levels.[44]

2.13. Statistics. All of the data are expressed as the mean ± standard deviation (SD). One way analysis of variance (ANOVA) with Bonferroni multiple comparison test was used with Sigma Stat (V.3.5 Systat Software Inc., San Jose, CA, USA). A p value < 0.05 is considered statistically significant.

3. RESULTS AND DISCUSSION

3.1. Polymer Synthesis and Characterization. The synthesis of pPEGMA-PCL-ss-PCL-pPEGMA triblock copolymers was carried out in three steps as per the synthesis scheme in Figure 1. First, ring opening polymerization of ε-caprolactone was carried out with cystamine as initiator in the presence of tin(II) 2-ethylhexanoate as a catalyst. The ^{1}H NMR spectrum (Supporting Information, Figure S1A) confirmed the structure of polycaprolactone diol with a cystamine core. In the ^{1}H NMR spectrum, multiplet peaks at δ 1.38 corresponding to central methylene units of the caprolactone unit ($-OCH_2CH_2\boldsymbol{CH_2}CH_2CH_2CO-$), multiplet at δ 1.62 corresponding to methylene groups of the caprolactone unit ($-OCH_2\boldsymbol{CH_2}CH_2\boldsymbol{CH_2}CH_2CO-$), and triplet peak at δ 2.28 corresponding to methylene groups attached to carbonyl group in polycaprolactone unit ($-OCH_2CH_2CH_2CH_2\boldsymbol{CH_2}CO-$) confirmed the presence of polycaprolactone units in the polymer. The triplet peak at δ 2.8 corresponding to methylene units attached to disulfide in cystamine ($-NHCH_2\boldsymbol{CH_2}$-SS-$\boldsymbol{CH_2}CH_2NH-$) and another triplet peak at δ 3.55 corresponding to methylene units attached to nitrogen in cystamine ($-NH$-$\boldsymbol{CH_2}CH_2$-SS-$CH_2\boldsymbol{CH_2}$-$NH-$) confirmed the successful synthesis of polycaprolactone diol (HO-PCL-ss-PCL-OH). The molecular weight (M_n) of the polymer was determined by GPC and found to be 20 400 Da as shown in Supporting Information, Figure S2a.

In the second step, the PCL macroinitiator was synthesized by reacting the terminal −OH groups of polycaprolactone with α-bromoisobutyryl bromide in the presence of trimethylamine in dry dichloromethane. The synthesized macroinitiator was characterized by ^{1}H NMR (Supporting Information, Figure S1B). The ^{1}H NMR spectrum of the PCL macroinitiator showed a new peak at δ 1.96 ppm due to the attachment of α-bromoisobutyryl bromide in the terminal. Also, shifting of the peak corresponding to the terminal methylene group from 3.55 to 4.18 also confirmed the conversion of PCL diol to PCL macroinitiator. On the basis of integration in the ^{1}H NMR spectra of the PCL macroinitiator, it was observed that both hydroxyl end groups in the polycaprolactone diol were functionalized by α-bromoisobutyryl bromide where the degree of functionalization was calculated as two.

In the third step, pPEGMA-PCL-ss-PCL-pPEGMA triblock copolymers were synthesized from the PCL macroinitiator using ATRP. The PCL macroinitiator, in the presence of CuBr

DOI: 10.1021/acsami.5b01731
ACS Appl. Mater. Interfaces 2015, 7, 9211−9227

and PMDETA, initiated controlled free radical catalyzed polymerization of PEGMA with different molar ratios in dry toluene under nitrogen atmosphere to generate a series of amphiphilic triblock copolymers with varying hydrophilic to hydrophobic content. For ATRP reaction, the ratio of CuBr/PMDETA was taken as 1:1 for the higher rate constant. The PCL macroinitiator/CuBr/PMDETA ratio was taken as 1:2:2 because the ATRP reaction was initiated from two end functional groups of the macroinitiator, and hence, double the molar equivalent of catalysts was required. The triblock copolymers were characterized by ^{1}H NMR, GPC, and FTIR (Supporting Information, Figures S1C, S2, and S3, respectively).

In the proton NMR spectrum, a single broad peak at δ 3.6 ppm corresponds to the $-OCH_2$ group of PEGMA chains in the triblock copolymer. The FTIR spectrum showed a broad peak in the range of 3400−3500 cm^{-1} due to the hydroxyl group of PEGMA and another peak at 1100 cm^{-1} due to the C−O−C stretching of PEGMA, which confirmed the presence of PEGMA in the polymer.

The molecular weights of polymers were determined using GPC and ^{1}H NMR and are depicted in Table 3.

It was observed that M_n determined by GPC was higher than that determined using NMR. The difference could arise from the fact that molecular weight in GPC has been calculated relative to the polystyrene standards used for calibration. Also, the hydrodynamic volume of the PEGylated copolymers is quite different from that of the standards leading to the difference of calculated and actual molecular weights. A similar observation has been reported in the literature.[45]

3.2. DTT-Triggered Degradation of pPEGMA-PCL-ss-PCL-pPEGMA Polymers. To establish the susceptibility of disulfide linkage in the polymer backbone to reductive degradation, the copolymers (P6−P24) were treated with the redox reagent DTT (10 mM) in DMSO solution. DTT is a very strong reducing agent and cleaves disulfide linkages of the polymer to form two sulfhydryl moieties as shown in Figure 2. Reducing agents like DTT/GSH form negatively charged thiolate species which are responsible for the reduction of disulfides. The thiolates attack disulfide bonds and convert them into thiol groups via thiol−disulfide exchange reactions. The degradation products of the redox reaction were characterized by ^{1}H NMR and GPC (Supporting Information, Figure S4). It was observed that molecular weights of all of the polymers were reduced to approximately half of their original molecular weight after DTT degradation as shown in Table 3.

3.3. Conjugation of Folic Acid to pPEGMA-PCL-ss-PCL-pPEGMA. Folic acid was conjugated to the pendant hydroxyl group of the triblock copolymer via the DCC-NHS coupling method. In this reaction, γ-carboxylic acid of folic acid was first activated by DCC-NHS, and then activated folic acid was reacted with the pendant hydroxyl groups of the triblock copolymer. Unreacted folic acid was removed by dialysis and lyophilized. Conjugation of folic acid was determined by FTIR. The FTIR spectrum showed N−H stretching at 3300 cm^{-1}, and the OH peak of PEG chains was reduced after folic acid conjugation (Supporting Information, Figure S3).

3.4. Size and Morphological Characterization of Polymer Nanoparticles. Self-assembled polymer nanoparticles were prepared by nanoprecipitation in aqueous medium. It was observed that the polymers self-assembled to form nanoparticles of different size and morphological variation based on the molecular weight fraction of the PEG blocks in the triblock copolymers. As the hydrophilic fraction in the triblock copolymer increased, the morphology of polymer nanoparticles changed from vesicular to micellar structure.

The hydrodynamic size and zeta potential of all nanoparticles (P6−P24) are shown in Table 4. P12 formed polymeric vesicles

Table 4. Hydrodynamic Size and Zeta Potential of Polymeric Nanoparticles[a]

polymers	size (nm)	PDI	ζ (mV)	hydrophilicity (%) (from NMR)
P6	141.7 ± 1.8	0.080	−18.8 ± 1.8	2.97
P9	175.27 ± 2.1	0.095	−21.8 ± 1.8	11.40
P12	186.2 ± 1.6	0.240	−16.4 ± 2.2	17.99
P24	156 ± 2.3	0.212	−22.8 ± 2.8	39.63

[a]Mean ± SD, n = 3.

(polymersomes) with hydrodynamic diameters of ∼186 ± 1.6 nm and zeta potential of ∼−16 ± 2.2 mV. The observed negative zeta potential of the polymeric nanoparticles can be attributed to the presence of ester linkages in the polycaprolactone units. Thus, in addition to steric stabilization due to PEG, the particle dispersions were also stabilized by electrostatic repulsion. DLS showed unimodal distribution of particle size with narrow polydispersity index (PDI 0.240). The SEM image of the P12 polymer showed a particle size of ∼150 nm, while TEM revealed the core−shell morphology of polymersomes as shown in Figure 3.

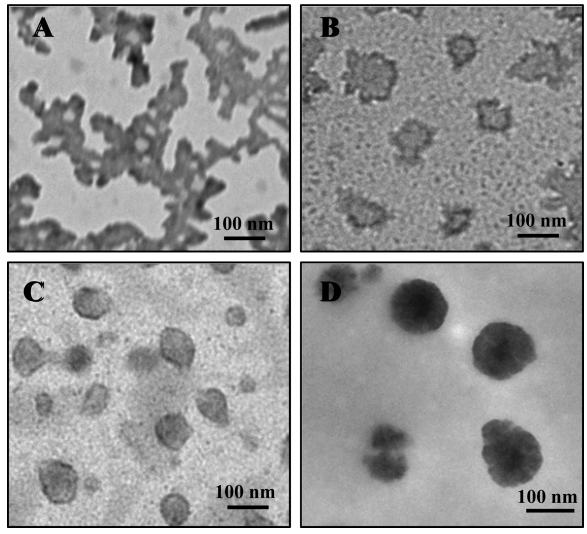

Figure 3. TEM image of polymer nanoparticles (A) P6, (B) P9, (C) P12, and (D) P24.

The TEM images in Figure 3 depict the effect of polymer composition on nanoparticle structures. The polymers formed different morphologies as the PEGMA ratio changed from 2.97% to 39.63%. P9 and P12 showed vesicular core−shell morphology, while P24, having a relatively large PEG content, formed micelles. It is widely known that the hydrophilic/hydrophobic ratio drives the self-assembly of the block copolymers in aqueous medium.[7] It was observed that the colloidal suspension of polymers with low PEG content (P6 and P9) appeared as aggregates (Figure 3A and B). Figure 3B shows phase separation of the polymer aggregates into hydrophobic and hydrophilic regions, with hydrophobic areas

DOI: 10.1021/acsami.5b01731
ACS Appl. Mater. Interfaces 2015, 7, 9211−9227

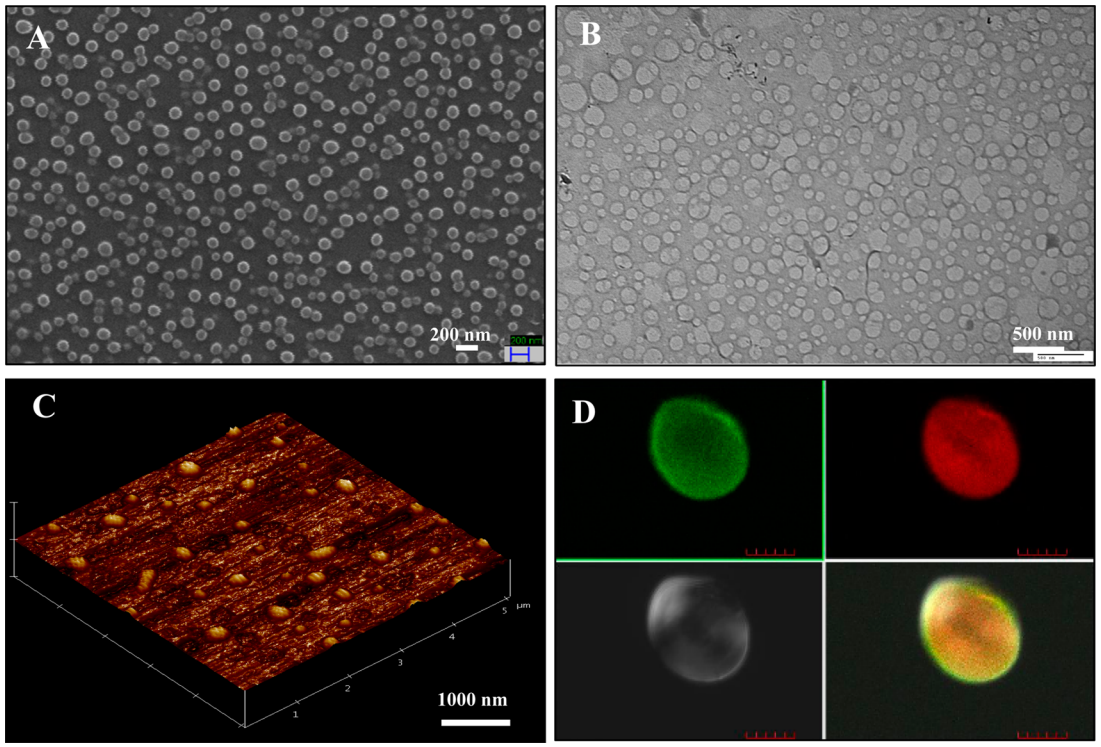

Figure 4. Doxorubicin loaded P12 polymersomes (A) SEM, (B) TEM, (C) AFM, and (D) dual dye loaded P12 polymersomes as observed in CLSM.

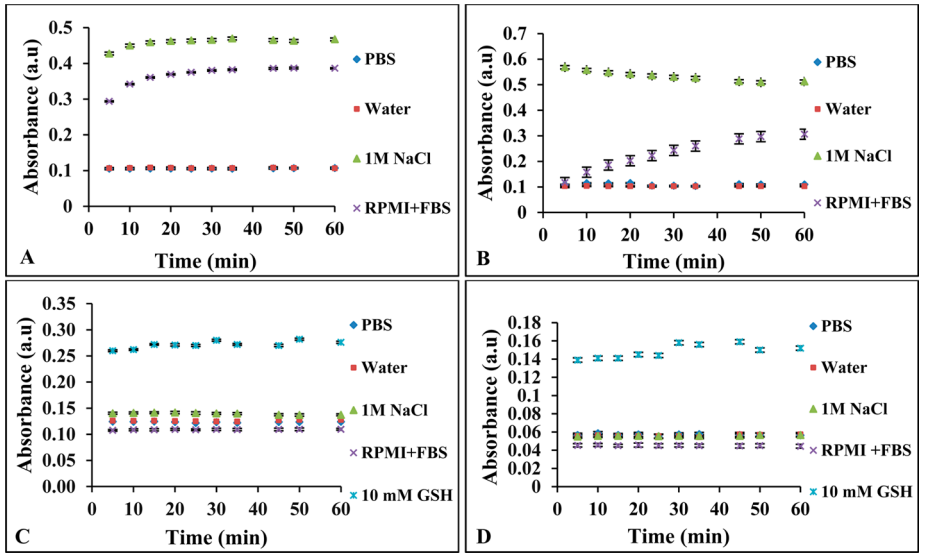

Figure 5. Colloidal stability of nanoparticle dispersions in different media: (A) P6, (B) P9, (C) P12, and (D) P24. (Mean ± SD, n = 3.)

appearing dark while the hydrophilic part appears as bright cores against the dark background. With increase in PEG content, better stabilization of self-assembled nanoparticles became apparent. The polymer with higher hydrophilic content (P12) formed polymersomes in aqueous medium. The core–shell morphology is shown in Figure 3C, which depicts the dark hydrophobic shell of the vesicles, and the bright aqueous lumen resulted in more robust structures. P24 with a PEG content of ~40% formed micelles (Figure 3D), where a dark hydrophobic core and hydrophilic corona are distinguishable.

Vesicular structures formed by P12 were also observed in the TEM micrograph of the doxorubicin loaded polymer nanoparticle (Figure 4B). A biconcave erythrocyte-like appearance can be seen in Figure 4B, which arises from the removal of water from the vesicle interior during drying, while sample preparation leaves a deflated appearance. Figure 4C depicts the AFM micrograph of P12 particles where smooth spherical morphology can be discerned.

The core–shell structure of polymer vesicles formed by the folic acid conjugated P12 polymer was confirmed by confocal laser scanning microscopy by simultaneous encapsulation of fluorescent dyes PI (hydrophilic dye) and FITC (hydrophobic dye). FITC was localized to the shell of the polymeric vesicles, while PI was observed in the interior, thus illustrating the core–

DOI: 10.1021/acsami.5b01731
ACS Appl. Mater. Interfaces 2015, 7, 9211–9227

shell morphology of the polymersomes as shown in Figure 4D. The z-section of polymersomes clearly showed the core−shell nature of the polymersomes (Supporting Information, Figure S5).

3.5. Colloidal Stability. The stability of nanoparticles is important for the clinical use of these nanocarriers. It is important to establish the stability of nanoparticles in dispersions as agglomeration of the nanoparticles changes the nature of cell−nanoparticle interactions.[46] To avoid complications due to the aggregation of polymer nanocarriers, the colloidal stability of polymeric nanoparticles in different media was studied by turbidimetry.[46] Steric stabilization was achieved by PEGylation of the nanoparticle surface. This stabilizing effect was clearly evident when nanoparticles were incubated with different dispersion media as shown in Figure 5.

The polymers with a relatively large PEG content, viz. P12 and P24, were stable in all media tested, including 1 M NaCl as well as the cell culture medium However, P6 and P9 were aggregated in 1 M NaCl and in the cell culture medium due to the inadequate steric shielding by the PEG coating. P12 and P24 nanoparticles were additionally tested in 10 mM GSH, since GSH is a naturally occurring reducing agent present in the cytosol.[26] A rapid increase in turbidity was observed in this environment, indicating the degradation and subsequent aggregation of nanoparticles under the influence of GSH.

Colloidal stability of P12 polymersomes was also studied by measuring hydrodynamic diameter using DLS. In PBS, there was no variation in the size of the polymersomes over a period of 24 h, whereas in the presence of 10 mM GSH, particle size increased from 170.6 to 226 nm after 1 h. The size as well as polydispersity increased on each subsequent measurement until 24 h when large aggregates were formed, as shown in Figure 6. The TEM image of aggregated polymeric nanoparticles after treatment with 10 mM GSH is provided in Supporting Information, Figure S6.

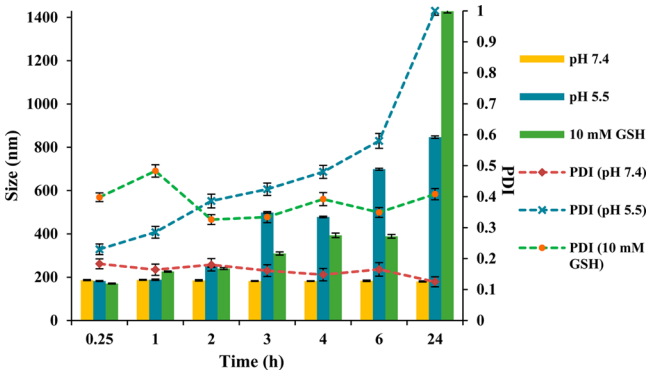

Figure 6. Size variation of P12 polymersomes in different media (pH 7.4, pH 5.5, and 10 mM GSH) (mean ± SD, n = 3).

3.6. Protein Adsorption. A major challenge in nanoparticle drug delivery is the opsonization and phagocytic uptake of nanoparticles during systemic circulation. The most abundant protein in the blood, albumin, gets easily adsorbed on the surface of hydrophobic or charged particles. PEGylation is a widely adopted strategy to prevent adsorption of serum proteins.[29,31] Hydrophilic PEG chains provide steric protection from protein adsorption rendering the particles invisible to the phagocytic cells (macrophages of the reticuloendothelial (RES) cells and dendritic cells). In this study, we observed decreased protein adsorption with increase in PEG content in the block copolymers as shown in Figure 7. Micelles prepared from P24

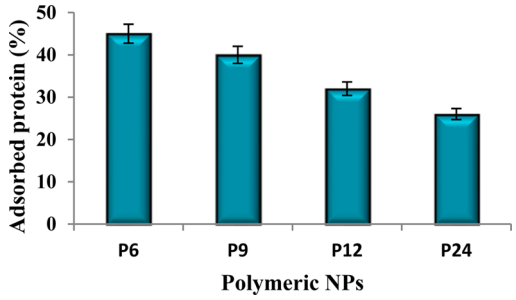

Figure 7. Extent of protein (BSA) adsorption with polymeric NPs P6−P24. (Mean ± SD, n = 3.)

showed least BSA adsorption compared to that of particles prepared from the other polymers. The extent of protein adsorption was in the order P6 > P9 > P12 > P24. On the basis of morphology, stability, and protein adsorption studies, P12 polymersomes were chosen for drug loading, drug release, and *in vitro* and *in vivo* studies.

3.7. Blood Compatibility Studies. For the intravenously administrated formulation, it is necessary to study the blood compatibility of nanocarriers. The interaction of P12 polymersomes with blood was analyzed by hemolysis and coagulation studies.

3.7.1. Hemolysis Study. Hemolysis study of Tri-ss-NPs was determined by UV−visible spectrophotometry at 540 nm after incubating polymersomes (concentration of 0.5- 2 mg/mL) with RBCs. Hemolysis levels less than 20% are considered acceptable for nanoparticle formulations.[47,48]

P12 polymersomes exhibited low hemolytic activity for the concentrations studied. At a concentration of 1 mg/mL, 1.91% hemolysis was observed, while with 2 mg/mL, 6.5% hemolysis occurred as shown in Figure 8. Thus, the polymersomes showed no significant blood hemotoxicity and hence are biocompatible with respect to hemolysis.

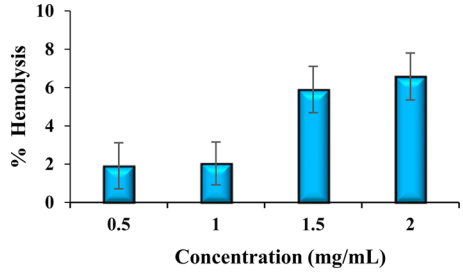

Figure 8. Hemolytic activity of P12 polymersomes (mean ± SD, n = 3).

3.7.2. Coagulation Studies. During blood circulation, nanoparticles can interact with coagulation factors and alter the coagulation pathway. A PT and aPTT study represents extrinsic and intrinsic pathways of coagulation.[49,50] A PT and aPTT study was performed to evaluate the interaction of the polymersomes with coagulation factors. The acceptable range for PT and aPTT is 11−14 s and 27−40 s, respectively.[40] With Tri-ss-NPs, PT values ranged from 12.8 ± 0.15 s to 13.2 ± 0.05 s, while aPTT values ranged from 25.8 ± 0.15 s to 27.1 ± 0.10 s for polymersome concentrations of 100−500 μg/mL, as shown

DOI: 10.1021/acsami.5b01731
ACS Appl. Mater. Interfaces 2015, 7, 9211−9227

in Figure 9. Thus, this study demonstrates that the polymersomes do not cause activation of coagulation pathways and are biocompatible with respect to coagulation pathways.

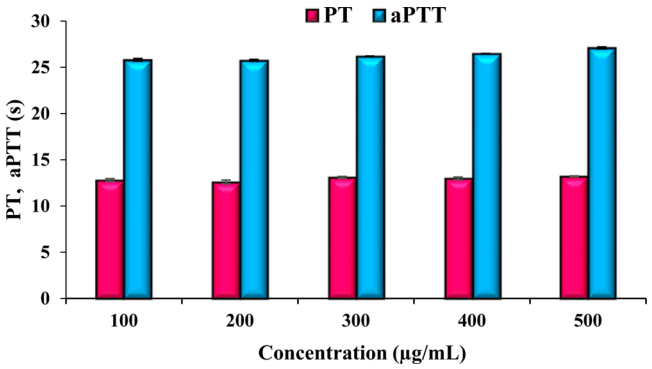

Figure 9. PT and aPTT assay of P12 polymersomes (mean ± SD, n = 3).

3.8. Drug Loading and Release. Doxorubicin hydrochloride was loaded in the polymersomes at pH 10.5 as per Sanson et al.[42] At pH ∼10.5, doxorubicin hydrochloride is converted to hydrophobic doxorubicin free base and is efficiently partitioned out of the aqueous external medium into the hydrophobic compartment of the polymersomes, leading to higher drug loading content of ∼21%.[42]

Drug release was studied in different media including neutral and acidic pH, in the presence and absence of GSH to simulate cytosolic and endocytic environments in cancer cells. 12.68% drug release was observed at 24 h in pH 7.4, while 25.78% drug was released in pH 5.5 under similar conditions (Figure 10).

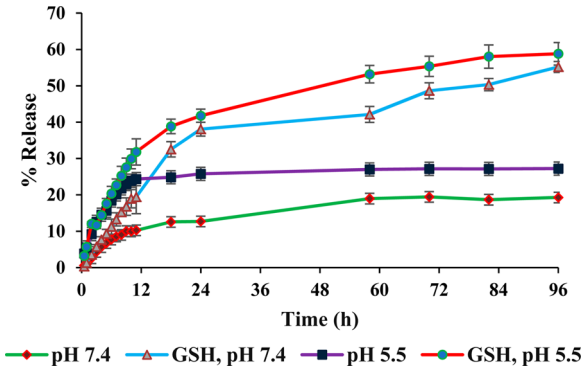

Figure 10. Drug release profile of polymersomes in pH 7.4 and in pH 5.5 with and without 10 mM GSH (mean ± SD, n = 3).

The presence of GSH in the release medium further accelerated drug release due to the breakage of disulfide linkage in the polymer backbone by reversible disulfide−thiol exchange reactions between the disulfide group of polymer and the thiol group of GSH. GSH destabilizes polymersome nanostructure because of which the encapsulated drug is released in the external medium. Drug release of 38.07% and 41.77% was obtained at 24 h in pH 7.4 and 5.5, respectively, in the presence of GSH. Thus, due to redox sensitive linkages in the polymersomes, efficient drug release may be anticipated in intracellular environment in cancer cells.

3.9. Trastuzumab Conjugation with Polymersomes and Its Characterization. Zeta potential, EDX, and XPS were used to characterize trastuzumab conjugation on the polymersomes. Zeta potential of the polymersomes before and after trastuzumab conjugation was determined using DLS and is shown in Table 5. After trastuzumab conjugation, the zeta potential of NPs shifted to the positive side, which can be attributed to the positive charge of trastuzumab, indicating the successful conjugation of trastuzumab on the polymersomes surface. EDX results also confirmed trastuzumab conjugation based on increased nitrogen content in the samples as shown in Table 5.

Table 5. Zeta Potential and Nitrogen Content of Targeted Polymersomes[a]

targeted polymersomes	zeta potential[a]	nitrogen content % (EDX)
Tri-ss-NPs	−28.5 ± 2.2	0.80
Tri-ss-Dox-NPs	−20.2 ± 1.2	8.43
Tri-ss-FA-Dox-NPs	−16.4 ± 0.90	13.20
Tri-ss-Her-Dox-NPs	−4.40 ± 0.56	14.97
Tri-ss-FA-Her-Dox-NPs	−7.11 ± 0.94	21.78

[a]Mean ± SD, n = 3.

The surface chemistry of polymersomes was studied using XPS to confirm trastuzumab conjugation on the polymersomes as shown in Figure 11. The trastuzumab conjugated polymer showed a nitrogen peak in the binding energy region of 398−400 eV, which can be attributed to 1726 nitrogens present in the trastuzumab molecule.

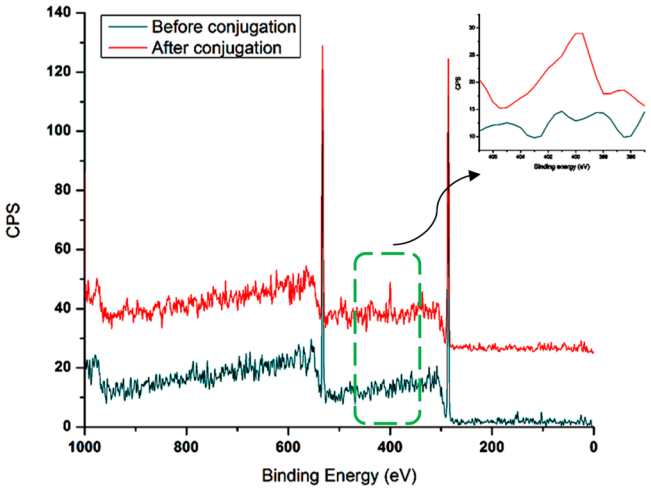

Figure 11. XPS spectra of polymersomes before and after trastuzumab conjugation. XPS spectra showed a strong peak in the binding energy range (N, 1s) 398−400 eV in trastuzumab conjugated polymersomes.

3.10. Cell Culture Studies. *3.10.1. Cell Viability Studies.* Cell viability of MCF-7 on treatment with nanoparticle dispersions was determined by the MTT assay, as shown in Figure 12. Conversion of the pale yellow MTT dye to purple formazan crystals by the mitochondrial dehydrogenase enzyme present in metabolically active cells is quantified as a measure of percent cell viability. At the highest concentration of P12 polymer used in the study (2 mg/mL), 95.91% cell viability was observed. Thus, the P12 polymer was found to be biocompatible in the concentration range 0.5−2.0 mg/mL.

3.10.2. Cellular Uptake Studies Using Confocal Laser Scanning Microscopy. Cellular uptake of nontargeted polymersomes (Tri-ss-Dox-NPs) and targeted polymersomes, folic acid conjugated polymersomes (Tri-ss-FA-Dox-NPs),

DOI: 10.1021/acsami.5b01731
ACS Appl. Mater. Interfaces 2015, 7, 9211−9227

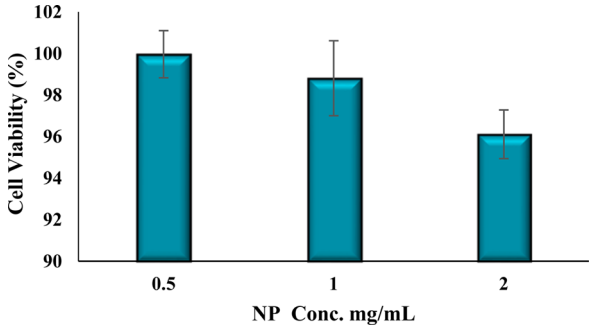

Figure 12. Cell viability of polymersomes (P12) (Tri-ss-NPs) by the MTT assay in the MCF-7 breast cancer cell line. (Mean ± SD, n = 3.)

trastuzumab conjugated polymersomes (Tri-ss-Her-Dox-NPs), and both folic acid and trastuzumab conjugated polymersomes (Tri-ss-FA-Her-Dox-NPs), were evaluated for their targeting efficiency in BT474, MCF-7, and L929 cell lines. In MCF-7 cells, folate FRα receptors are overexpressed, while in BT474 cells, HER2 receptors are overexpressed.[51,52]

As shown in Figure 13, BT474 and MCF-7 cancer cells showed higher uptake of Tri-ss-FA-Dox-NPs through folate mediated endocytosis leading to higher accumulation in the cells. Similarlarly, Tri-ss-Her-Dox-NPs also showed higher cellular uptake as compared to that of nontargeted polymersomes. Dual targeted Tri-ss-FA-Her-Dox-NPs showed even higher doxorubicin fluorescence intensity as compared to that of Tri-ss-FA-Dox-NPs and Tri-ss-Her-Dox-NPs indicating higher cellular uptake as compared to that of cells treated with single targeted/nontargeted polymersomes. Higher accumulation of Tri-ss-FA-Her-Dox-NPs in the cells can be attributed to folate FRα and HER2 receptor mediated endocytosis of polymersomes.

L929 cell line is a noncancerous fibroblast cell line,[53] which does not express FRα or HER2 receptors, and hence, low fluorescence intensity was observed with Tri-ss-FA-Dox-NPs, Tri-ss-Her-Dox-NPs, and Tri-ss-FA-Her-Dox-NPs. The fluorescence intensity was low and similar in all four types of polymersomes showing nonspecific cellular uptake of polymersomes.

3.10.3. Cellular Uptake Studies Using Flow Cytometry. Figure 14 demonstrates the cellular uptake of nontargeted and targeted polymersomes in BT474, MCF-7, and L929 cell lines to evaluate the targeting efficiency of folate and/or trastuzumab conjugated polymersomes. Tri-ss-FA-Dox-NPs and Tri-ss-Her-Dox-NPs showed ∼10-fold increase in median fluorescence intensity as compared to that of nontargeted NPs (Tri-ss-Dox-NPs). This increment in fluorescence intensity is due to the folate/trastuzumab mediated enhanced endocytosis of NPs. Tri-ss-FA-Her-Dox-NPs showed ∼22-fold increase in median fluorescence intensity as compared to that of nontargeted Tri-ss-Dox-NPs, indicating the higher targeting efficiency of Tri-ss-FA-Her-Dox-NPs as compared to that of Tri-ss-Dox-NPs as well as single targeted Tri-ss-FA-Dox-NPs and Tri-ss-Her-Dox-NPs. In L929 cells, low median fluorescence intensity was observed with all four types of polymersomes indicating the nonspecific cellular uptake of NPs. Thus, FACS cellular uptake studies corroborated with the confocal studies regarding the superior uptake of dual targeted polymersomes in cancer cells.

3.10.4. Annexin V-FITC Apoptosis Assay. The apoptotic and necrotic cells were distinguished from healthy cells by the Annexin V-FITC assay. Cells undergoing apoptosis expose

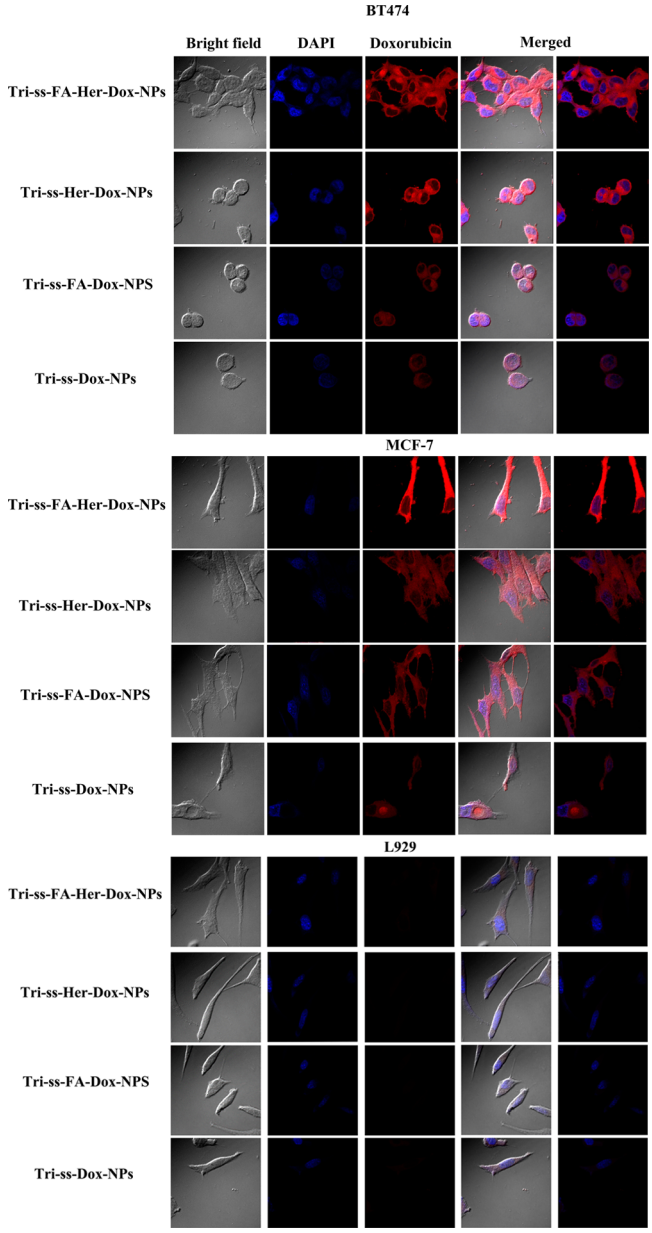

Figure 13. Cellular uptake of polymersomes by BT474, MCF-7, and L929 cell lines.

phosphatidylserine on their outer cell surface. Annexin V is a phospholipid binding protein which selectively binds to exposed phosphatidylserine in the presence of calcium and thus is able to detect apoptotic cells. Propidium iodide stains cells which lose cell membrane integrity and intercalates the DNA nonspecifically. Necrotic cells generally have damaged cell membranes and are stained with both Annexin V-FITC and propidium iodide. Apoptotic cells with their integral membrane do not take up propidium iodide and thus can be differentiated from necrotic cells. Healthy cells do not take up Annexin V-FITC or propidium iodide and thus can be differentiated from apoptotic and necrotic cells.[54]

As shown in Figure 15, in the case of BT474 and MCF-7 cells, untreated control cells were free from necrotic/apoptotic cells. Single targeted polymersomes (Tri-ss-FA-Dox-NPs and Tri-ss-Her-Dox-NPs) showed higher apoptotic and necrotic cells as compared to that of Tri-ss-Dox-NPs. The higher

DOI: 10.1021/acsami.5b01731
ACS Appl. Mater. Interfaces 2015, 7, 9211−9227

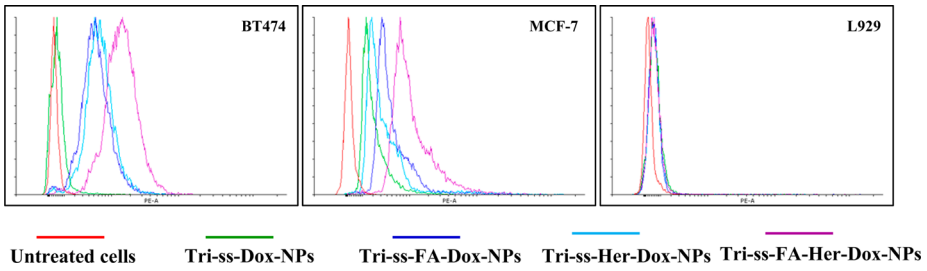

Figure 14. Cellular uptake of polymersomes in cell lines BT474, MCF-7, and L929 by FACS.

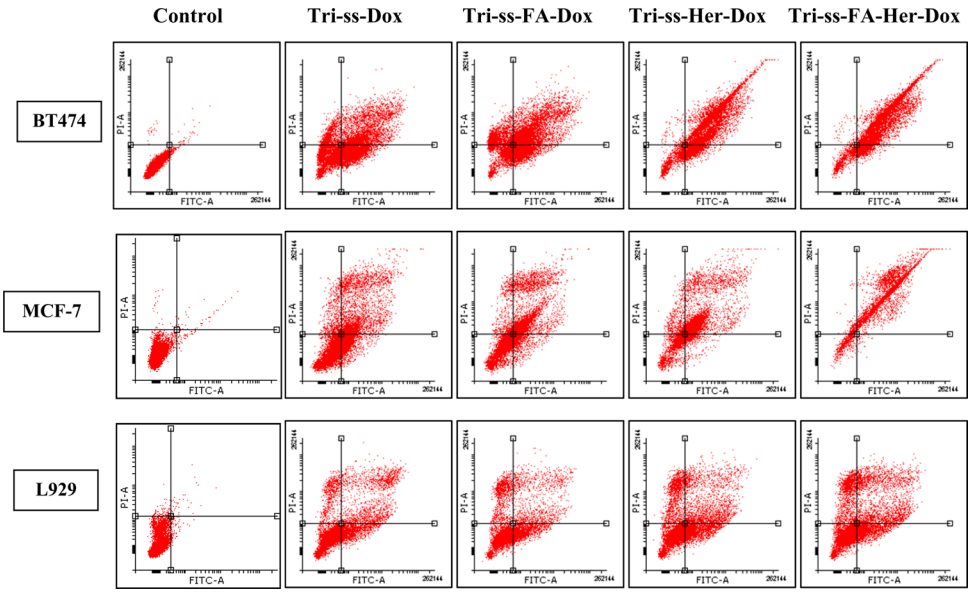

Figure 15. Annexin V-FITC apoptosis assay for the determination of apoptotic/necrotic cells in BT474, MCF-7, and L929 cell lines using flow cytometry.

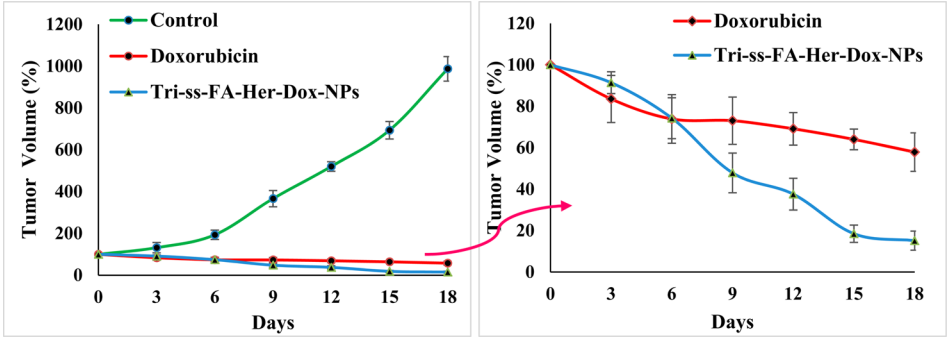

Figure 16. Evaluation of the *in vivo* efficacy of Tri-ss-FA-Her-Dox-NPs in EAT bearing Swiss albino mice with respect to plain doxorubicin and the control. Data are shown as the mean ± SEM, $n = 6$.

percent of apoptotic and necrotic cells in Tri-ss-FA-Dox-NPs and Tri-ss-Her-Dox-NPs treated cells can be ascribed to FRα and HER2 receptor mediated endocytosis. Dual targeted polymersomes (Tri-ss-FA-Her-Dox-NPs) with folate as well as trastuzumab showed even higher apoptotic and necrotic cells as compared to that of folate/trastuzumab targeted polymersomes in BT474 and MCF-7 cells. The higher targeting efficiency of dual targeted polymersomes resulted in higher cellular doxorubicin concentration, which led to higher apoptosis in cancer cells.

L929 cells treated with all the polymersomes showed results similar to those of nontargeted polymersomes indicating lower apoptosis in noncancerous cells as compared to that of BT474 and MCF-7 cancer cells. This can be ascribed to the absence of folate FRα and HER2 receptors in L929 cells.

3.11. Animal Studies. EAT is a widely used model for cancer studies. It is characterized by undifferentiated carcinoma with high transplantable capability, no-regression, rapid proliferation rate, and lack of tumor-specific transplantation antigen.[55] The cancer cells in the EAT tumor overexpress folate and HER2 receptors,[56−58] and hence, the EAT tumor model was selected for our experiments.

3.11.1. Determination of In Vivo Antitumor Efficacy. Antitumor efficacy of Tri-ss-FA-Her-Dox-NPs was investigated in Swiss albino mice bearing EAT. When the tumor volumes

DOI: 10.1021/acsami.5b01731
ACS Appl. Mater. Interfaces 2015, 7, 9211−9227

reached 200−250 mm,[3] mice were administered with Tri-ss-FA-Her-Dox-NPs and free doxorubicin.

As shown in Figure 16, the control group showed a progressive increase in tumor size up to 1000%, i.e., about 10 times in size as compared to the initial size of the tumor. Doxorubicin treated mice showed moderate antitumor effect with ∼42% reduction in tumor volume, whereas Tri-ss-FA-Her-Dox-NPs showed statistically significant excellent antitumor effects as compared to that of the control and free doxorubicin treated mice with ∼85% reduction in tumor volume.

The enhanced antitumor activity of Tri-ss-FA-Her-Dox-NPs can be attributed to longer blood circulation of polymersomes due to pendant PEG chains, potential higher accumulation in the tumor via the dual targeting approach, and GSH triggered intracellular release of doxorubicin due to the presence of disulfide linkage in the polymer backbone. These results indicated the superior antitumor efficacy of dual targeted polymersomes with high drug loading content and glutathione sensitive linkage in the polymer backbone

3.12. Toxicological Studies. *3.12.1. Histopathology.* Further investigation of the antitumor efficacy of Tri-ss-FA-Her-Dox-NP treated mice was carried out using histopathological analysis of the tumor, as shown in Figure 17. Tumor sections of control mice showed active proliferation with viable tumor cells, whereas doxorubicin treated mice showed viable tumors in the periphery and necrosis areas in the center. Tri-ss-FA-Her-Dox-NPs showed a large necrosis area with very few viable cells. Thus, the tumor histopathological study agrees with the tumor regression study regarding the enhanced antitumor efficacy of Tri-ss-FA-Her-Dox-NPs.

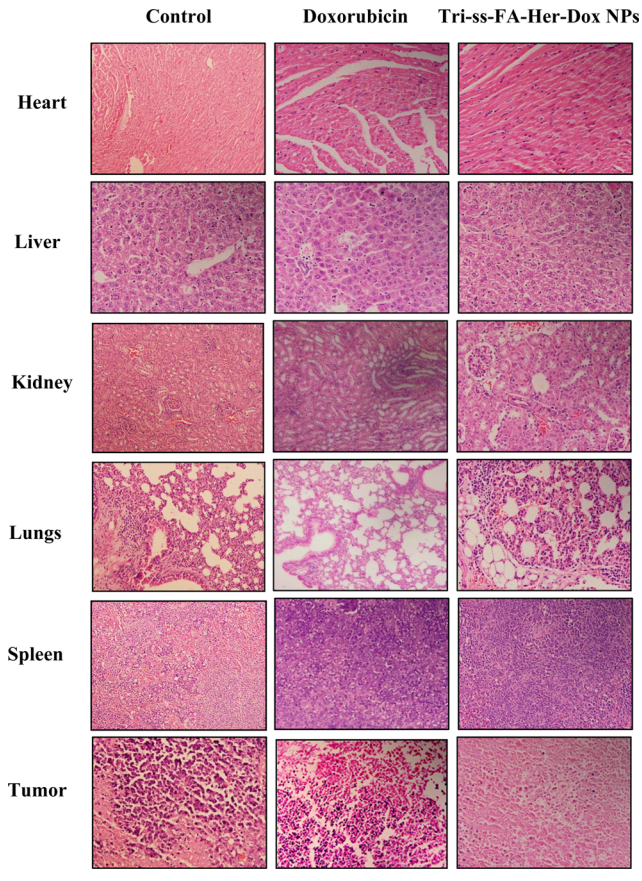

Figure 17. Histopathological slides of vital organs of EAT bearing Swiss albino mouse heart, liver, kidney, lungs, spleen, and tumor.

To determine the effect of the formulations on vital organs such as the heart, liver, kidney, lungs, and spleen, the histopathology of these organs was analyzed, as shown in Figure 17. Free doxorubicin treated mouse heart showed cardiomyocyte swelling, nuclear pyknosis, and significant cytoplasmic vacuolization indicating the cardiotoxicity of doxorubicin. Tri-ss-FA-Her-Dox-NPs, however, showed mild cardiomyocyte swelling with mild cytoplasmic vacuolization indicating cardiac biocompatibility.

The liver section showed foci of spotty necrosis and Kupffer cell prominence in doxorubicin treated mice indicating hepatotoxity. In the case of the kidney, significant tubular damage was observed with doxorubicin treated mice. Tri-ss-FA-Her-Dox-NPs showed histology similar to that of the control indicating nontoxicity to these organs.

The nontoxicity of Tri-ss-FA-Her-Dox-NPs to these vital organs can be attributed to their dual targeting ability and redox responsiveness, which prevented drug release during circulation and allowed cancer specific targeting resulting in higher accumulation in tumor tissue.

3.12.2. Serum Biochemistry. The serum biochemistry was studied for investigating the toxicities of formulations to vital organs, the heart, liver, and kidney, in treated mice as shown in Table 6.

Table 6. Serum Biochemistry Results of EAT Bearing Swiss Albino Mice Treated with Free Doxorubicin and Tri-ss-FA-Her-Dox NPs[a]

parameter	control (PBS)	doxorubicin	Tri-ss-FA-Her-Dox NPs
total bilirubin (mg/dL)	0.28 ± 0.04	0.55 ± 0.06	0.38 ± 0.02
SGOT(AST) (IU/L)	66.84 ± 1.60	129.96 ± 3.60	72.48 ± 1.90
SGPT(ALT) (IU/L)	39.12 ± 1.86	80.16 ± 2.90	46.20 ± 1.60
alkaline phosphatase (IU/L)	140.04 ± 2.10	233.40 ± 6.10	150.36 ± 2.80
total protein (g/dL)	7.44 ± 0.12	6.72 ± 0.20	7.68 ± 0.22
albumin (g/dL)	4.20 ± 0.24	3.72 ± 0.16	3.72 ± 0.18
globulin (g/dL)	2.16 ± 0.16	1.80 ± 0.08	1.92 ± 0.02
A:G ratio	2.33 ± 0.22	2.48 ± 0.01	2.33 ± 0.10
total cholesterol (mg/dL)	130.44 ± 2.92	144.60 ± 1.72	138.96 ± 2.42
blood urea (mg/dL)	42.60 ± 2.40	80.76 ± 1.58	46.68 ± 1.22
S. creatinine (mg/dL)	0.36 ± 0.02	0.76 ± 0.02	0.43 ± 0.01
uric acid (mg/dL)	3.00 ± 0.16	7.68 ± 0.24	2.76 ± 0.26
calcium (mg/dL)	9.00 ± 0.24	8.28 ± 0.23	8.76 ± 0.22
phosphorus (mg/dL)	3.24 ± 0.18	4.08 ± 1.10	3.00 ± 0.28
CK-MB (IU/L)	2.00 ± 0.60	12.02 ± 1.60	4.10 ± 0.68

[a]All values are expressed as the mean ± SD, $n = 3$.

Cardiac toxicity was determined using creatine kinase MB (CK-MB) determination. CK-MB is a cardiac biomarker which is detected in serum after cardiac injury.[59] Doxorubicin treated mice showed significantly high levels of CK-MB in serum as compared to that in the control ($p < 0.05$) indicating cardiotoxicity. Tri-ss-FA-Her-Dox-NP treated mice showed statistically insignificant difference in CK-MB values as compared to that of the control ($p > 0.05$) indicating nontoxicity to cardiac tissues. Thus, the cardiotoxity of

DOI: 10.1021/acsami.5b01731
ACS Appl. Mater. Interfaces 2015, 7, 9211−9227

doxorubicin was overcome by the pPEGMA-PCL-ss-PCL-pPEGMA nanosystem.

Liver toxicity of the formulations was determined using liver specific enzymes such as alanine transaminases (ALT), aspartate transaminases (AST), and alkaline phosphatase (ALP). Doxorubicin treated mice showed a significant increase in ALT, AST, and ALP levels as compared to those of the control ($p < 0.05$), whereas Tri-ss-FA-Her-Dox-NP treated mice showed statistically insignificant elevation in their levels indicating nontoxicity to the liver. Kidney parameters like blood urea, creatinine, and uric acid levels were also higher in the case of doxorubicin treated mice as compared to that of the control, whereas Tri-ss-FA-Her-Dox-NPs showed levels of these biomarkers similar to those of the control indicating nontoxicity to the kidney.

Thus, we were able to achieve better antitumor efficacy using Tri-ss-FA-Her-Dox-NPs with reduced toxicities associated with doxorubicin (cardiotoxicity, hepatotoxicity, and nephorotoxicity).

4. CONCLUSIONS

In conclusion, the redox responsive biocompatible polymersomes exhibited core−shell morphology and can be utilized as a dual drug carrier as demonstrated in the CLSM study, which showed simultaneous compartmentalization of hydrophobic and hydrophilic dyes in the shell and lumen of the polymersomes. Biological evaluations such as the hemolysis study, coagulation studies, and the MTT cell viability assay demonstrated the biocompatible nature of these polymersomes, making them suitable for *in vivo* applications. Dual targeted polymersomes showed enhanced cellular uptake and apoptosis in breast cancer cell lines as compared to the single targeted and nontargeted polymersomes. *In vivo* studies in EAT bearing Swiss albino mice showed significant reduction in tumor size as compared to the free doxorubicin without any apparent toxicity to the heart, liver, or kidney, demonstrating the potential of these nanocarriers for intracellular drug delivery in cancer therapy.

■ ASSOCIATED CONTENT

Supporting Information

^{1}H NMR spectra of polycaprolactone diol, the polycaprolactone macroinitiator, and the pPEGMA-PCL-ss-PCL-pPEGMA triblock copolymer; FTIR spectra of the pPEGMA-PCL-ss-PCL-pPEGMA triblock copolymer and the folic acid conjugated pPEGMA-PCL-ss-PCL-pPEGMA triblock copolymer; GPC of polycaprolactone diol, pPEGMA-PCL-ss-PCL-pPEGMA triblock copolymers, and DTT degraded triblock copolymers; confocal image (z-section) of dye loaded polymersomes and the spectrophotometric (UV−visible) standard curve of doxorubicin. This material is available free of charge via the Internet at http://pubs.acs.org.

■ AUTHOR INFORMATION

Corresponding Author

*Tel: +91 1126591041. E-mail: veenak_iitd@yahoo.com.

Notes

The authors declare no competing financial interest.

■ ACKNOWLEDGMENTS

We are thankful to the Department of Biotechnology (DBT, India) for providing research funding (Project No. BT/PR13341/NNT/28/467/2009). A.K. is grateful to the Council of Scientific and Industrial Research, India for providing a senior research fellowship. A.K. thanks Dr. Archna Bansal and Professor Renu Saxena from All India Institute of Medical Science (AIIMS), New Delhi, for their help in CK-MB determination and coagulation studies, respectively. He also thanks Dr. Alok C. Bharti and Dr. Shyam B. Prasad from ICPO, Noida, India for their help in flow cytometry, Farhat Naz for her help in animal studies, and Dr. Nadeem Tanveer for his help with histopathological analysis.

■ REFERENCES

(1) Letchford, K.; Burt, H. A. Review of the Formation and Classification of Amphiphilic Block Copolymer Nanoparticulate Structures: Micelles, Nanospheres, Nanocapsules and Polymersomes. *Eur. J. Pharm. Biopharm.* **2007**, *65*, 259−269.

(2) Ganta, S.; Devalapally, H.; Shahiwala, A.; Amiji, M. A. Review of Stimuli-Responsive Nanocarriers for Drug and Gene Delivery. *J. Controlled Release* **2008**, *126*, 187−204.

(3) Kumari, A.; Yadav, S. K.; Yadav, S. C. Biodegradable Polymeric Nanoparticles Based Drug Delivery Systems. *Colloids Surf., B* **2010**, *75*, 1−18.

(4) Danhier, F.; Feron, O.; Preat, V. To Exploit the Tumor Microenvironment: Passive and Active Tumor Targeting of Nanocarriers for Anti-Cancer Drug Delivery. *J. Controlled Release* **2010**, *148*, 135−146.

(5) Panyam, J.; Labhasetwar, V. Biodegradable Nanoparticles for Drug and Gene Delivery to Cells and Tissue. *Adv. Drug Delivery Rev.* **2003**, *55*, 329−347.

(6) Rosler, A.; Vandermeulen, G. W.; Klok, H. A. Advanced Drug Delivery Devices via Self-Assembly of Amphiphilic Block Copolymers. *Adv. Drug Delivery Rev.* **2012**, *64*, 270−279.

(7) Adams, M. L.; Lavasanifar, A.; Kwon, G. S. Amphiphilic Block Copolymers for Drug Delivery. *J. Pharm. Sci.* **2003**, *92*, 1343−1355.

(8) Discher, B. M.; Won, Y. Y.; Ege, D. S.; Lee, J. C. M.; Bates, F. S.; Discher, D. E.; Hammer, D. A. Polymersomes: Tough Vesicles Made from Diblock Copolymers. *Science* **1999**, *284*, 1143−1146.

(9) Discher, D. E.; Ahmed, F. Polymersomes. *Annu. Rev. Biomed. Eng.* **2006**, *8*, 323−341.

(10) Lee, J. S.; Feijen, J. Polymersomes for Drug Delivery: Design, Formation and Characterization. *J. Controlled Release* **2012**, *161*, 473−83.

(11) Storey, R. F.; Sherman, J. W. Kinetics and Mechanism of the Stannous Octoate Catalyzed Bulk Polymerization of ε-Caprolactone. *Macromolecules* **2002**, *35*, 1504−1512.

(12) Kowalski, A.; Libiszowski, J.; Biela, T.; Cypryk, M.; Duda, A.; Penczek, S. Kinetics and Mechanism of Cyclic Esters Polymerization Initiated with Tin (II) Octoate. Polymerization of ε-Caprolactone and L,L-Lactide Co-Initiated with Primary Amines. *Macromolecules* **2005**, *38*, 8170−8176.

(13) Chiefari, J.; Chong, Y.; Ercole, F.; Krstina, J.; Jeffery, J.; Le, T. P.; Mayadunne, R. T.; Meijs, G. F.; Moad, C. L.; Moad, G. Living Free-Radical Polymerization by Reversible Addition-Fragmentation Chain Transfer: The RAFT Process. *Macromolecules* **1998**, *31*, 5559−5562.

(14) Chong, Y.; Le, T. P.; Moad, G.; Rizzardo, E.; Thang, S. H. A More Versatile Route to Block Copolymers and Other Polymers of Complex Architecture by Living Radical Polymerization: the RAFT process. *Macromolecules* **1999**, *32*, 2071−2074.

(15) Matyjaszewski, K.; Xia, J. Atom Transfer Radical Polymerization. *Chem. Rev.* **2001**, *101*, 2921−2990.

(16) Wang, J. S.; Matyjaszewski, K. Controlled/Living Radical Polymerization. Atom Transfer Radical Polymerization in the Presence of Transition-Metal Complexes. *J. Am. Chem. Soc.* **1995**, *117*, 5614−5615.

(17) Xia, J.; Matyjaszewski, K. Controlled/Living Radical Polymerization. Atom Transfer Radical Polymerization Using Multidentate Amine Ligands. *Macromolecules* **1997**, *30*, 7697−7700.

DOI: 10.1021/acsami.5b01731
ACS Appl. Mater. Interfaces 2015, 7, 9211−9227

(18) Hawker, C. J.; Bosman, A. W.; Harth, E. New Polymer Synthesis by Nitroxide Mediated Living Radical Polymerizations. *Chem. Rev.* **2001**, *101*, 3661−3688.
(19) Kim, M. S.; Lee, D. S. Biodegradable and pH-Sensitive Polymersome with Tuning Permeable Membrane for Drug Delivery Carrier. *Chem. Commun.* **2010**, *46*, 4481−4483.
(20) Onaca, O.; Enea, R.; Hughes, D. W.; Meier, W. Stimuli-Responsive Polymersomes as Nanocarriers for Drug and Gene Delivery. *Macromol. Biosci.* **2009**, *9*, 129−139.
(21) Meng, F.; Hennink, W. E.; Zhong, Z. Reduction-Sensitive Polymers and Bioconjugates for Biomedical Applications. *Biomaterials* **2009**, *30*, 2180−2198.
(22) Balendiran, G. K.; Dabur, R.; Fraser, D. The Role of Glutathione in Cancer. *Cell Biochem. Funct.* **2004**, *22*, 343−352.
(23) Saito, G.; Swanson, J. A.; Lee, K. D. Drug Delivery Strategy Utilizing Conjugation via Reversible Disulfide Linkages: Role and Site of Cellular Reducing Activities. *Adv. Drug Delivery Rev.* **2003**, *55*, 199−215.
(24) Cui, C.; Xue, Y. N.; Wu, M.; Zhang, Y.; Yu, P.; Liu, L.; Zhuo, R. X.; Huang, S. W. Cellular Uptake, Intracellular Trafficking, and Antitumor Efficacy of Doxorubicin Loaded Reduction Sensitive Micelles. *Biomaterials* **2013**, *34*, 3858−3869.
(25) Sun, H.; Guo, B.; Cheng, R.; Meng, F.; Liu, H.; Zhong, Z. Biodegradable Micelles with Sheddable Poly(ethylene glycol) Shells for Triggered Intracellular Release of Doxorubicin. *Biomaterials* **2009**, *30*, 6358−6366.
(26) Cheng, R.; Feng, F.; Meng, F.; Deng, C.; Feijen, J.; Zhong, Z. Glutathione-Responsive Nano-Vehicles as a Promising Platform for Targeted Intracellular Drug and Gene Delivery. *J. Controlled Release* **2011**, *152*, 2−12.
(27) Bauhuber, S.; Hozsa, C.; Breunig, M.; Göpferich, A. Delivery of Nucleic Acids via Disulfide Based Carrier Systems. *Adv. Mater.* **2009**, *21*, 3286−3306.
(28) Lv, L. P.; Xu, J. P.; Liu, X. S.; Liu, G. Y.; Yang, X.; Ji, J. Disulfide Crosslinked Biomimetic Micelles: Formation, Thiol Reactivity and Cytotoxicity Behavior. *Macromol. Chem. Phys.* **2010**, *211*, 2292−2300.
(29) Otsuka, H.; Nagasaki, Y.; Kataoka, K. Pegylated Nanoparticles for Biological and Pharmaceutical Applications. *Adv. Drug Delivery Rev.* **2003**, *55*, 403−419.
(30) Riehemann, K.; Schneider, S. W.; Luger, T. A.; Godin, B.; Ferrari, M.; Fuchs, H. Nanomedicine- Challenge and Perspectives. *Angew. Chem., Int. Ed.* **2009**, *48*, 872−897.
(31) Gref, R.; Luck, M.; Quellec, P.; Marchand, M.; Dellacherie, E.; Harnisch, S.; Blunk, T.; Müller, R. H. 'Stealth' Corona-Core Nanoparticles Surface Modified by Polyethylene Glycol (PEG): Influences of the Corona (PEG Chain Length and Surface Density) and of the Core Composition on Phagocytic Uptake and Plasma Protein Adsorption. *Colloids Surf., B* **2000**, *18*, 301−313.
(32) Ruoslahti, E.; Bhatia, S. N.; Sailor, M. J. Targeting of Drugs and Nanoparticles to Tumors. *J. Cell Biol.* **2010**, *188*, 759−768.
(33) Hoang, B.; Reilly, R. M.; Allen, C. Block Copolymer Micelles Target Auger Electron Radiotherapy to the Nucleus of HER2 Positive Breast Cancer Cells. *Biomacromolecules* **2011**, *13*, 455−465.
(34) Balasubramanian, S.; Girija, A. R.; Nagaoka, Y.; Iwai, S.; Suzuki, M.; Kizhikkilot, V.; Yoshida, Y.; Maekawa, T.; Nair, S. D. Curcumin and 5-Fluorouracil-Loaded, Folate-and Transferrin-Decorated Polymeric Magnetic Nanoformulation: A Synergistic Cancer Therapeutic Approach, Accelerated by Magnetic Hyperthermia. *Int. J. Nanomed.* **2014**, *9*, 437−459.
(35) Yu, M. K.; Park, J.; Jon, S. Targeting Strategies for Multifunctional Nanoparticles in Cancer Imaging and Therapy. *Theranostics* **2012**, *2*, 3−44.
(36) Veeranarayanan, S.; Poulose, A. C.; Mohamed, M. S.; Varghese, S. H.; Nagaoka, Y.; Yoshida, Y.; Maekawa, T.; Kumar, D. S. Synergistic Targeting of Cancer and Associated Angiogenesis Using Triple-Targeted Dual-Drug Silica Nanoformulations for Theragnostics. *Small* **2012**, *8*, 3476−3489.
(37) Rao, J. P.; Geckeler, K. E. Polymer Nanoparticles: Preparation Techniques and Size-Control Parameters. *Prog. Polym. Sci.* **2011**, *36*, 887−913.
(38) Vauthier, C.; Bouchemal, K. Methods for the Preparation and Manufacture of Polymeric Nanoparticles. *Pharm. Res.* **2009**, *26*, 1025−1058.
(39) Fessi, H.; Puisieux, F.; Devissaguet, J. P.; Ammoury, N.; Benita, S. Nanocapsule Formation by Interfacial Polymer Deposition Following Solvent Displacement. *Int. J. Pharm.* **1989**, *55*, R1−R4.
(40) Lale, S. V.; Aswathy, R. G.; Aravind, A.; Kumar, D. S.; Koul, V. AS1411 Aptamer and Folic Acid Functionalized pH-Responsive ATRP Fabricated pPEGMA−PCL−pPEGMA Polymeric Nanoparticles for Targeted Drug Delivery in Cancer Therapy. *Biomacromolecules* **2014**, *15*, 1737−1752.
(41) Lale, S. V.; Goyal, M.; Bansal, A. K. Development of Lyophilization Cycle and Effect of Excipients on the Stability of Catalase During Lyophilization. *Int. J. Pharm. Invest.* **2011**, *1*, 214−221.
(42) Sanson, C.; Schatz, C.; Le Meins, J. F.; Soum, A.; Thévenot, J.; Garanger, E.; Lecommandoux, S. A Simple Method to Achieve High Doxorubicin Loading in Biodegradable Polymersomes. *J. Controlled Release* **2010**, *147*, 428−435.
(43) Mosmann, T. Rapid Colorimetric Assay for Cellular Growth and Survival: Application to Proliferation and Cytotoxicity Assays. *J. Immunol. Methods* **1983**, *65*, 55−63.
(44) Serfilippi, L. M.; Pallman, D. R.; Russell, B. Serum Clinical Chemistry and Hematology Reference Values in Outbred Stocks of Albino Mice from Three Commonly Used Vendors and Two Inbred Strains of Albino Mice. *J. Am. Assoc. Lab. Anim. Sci.* **2003**, *42*, 46−52.
(45) Mahajan, S.; Koul, V.; Choudhary, V.; Shishodia, G.; Bharti, A. C. Preparation and in Vitro Evaluation of Folate-Receptor-Targeted Spion-Polymer Micelle Hybrids for MRI Contrast Enhancement in Cancer Imaging. *Nanotechnology* **2013**, *24*, 015603.
(46) Petri-Fink, A.; Steitz, B.; Finka, A.; Salaklang, J.; Hofmann, H. Effect of Cell media on Polymer Coated Superparamagnetic Iron Oxide Nanoparticles (SPIONs): Colloidal Stability, Cytotoxicity, and Cellular Uptake Studies. *Eur. J. Pharm. Biopharm.* **2008**, *68*, 129−137.
(47) Amin, K.; Dannenfelser, R. M. In Vitro Hemolysis: Guidance for the Pharmaceutical Scientist. *J. Pharm. Sci.* **2006**, *95*, 1173−1176.
(48) Krzyzaniak, J. F.; Nuunnez, F. A. A.; Raymond, D. M.; Yalkowsky, S. H. Lysis of Human Red Blood Cells. Comparison of in Vitro and in Vivo Hemolysis Data. *J. Pharm. Sci.* **1997**, *86*, 1215−1217.
(49) Gulati, N.; Rastogi, R.; Dinda, A. K.; Saxena, R.; Koul, V. Characterization and Cell Material Interactions of Pegylated PNIPAAM Nanoparticles. *Colloids Surf., B* **2010**, *79*, 164−173.
(50) Ilinskaya, A. N.; Dobrovolskaia, M. A. Nanoparticles and the Blood Coagulation System. Part II: Safety Concerns. *Nanomedicine* **2013**, *8*, 969−981.
(51) Nahire, R.; Haldar, M. K.; Paul, S.; Mergoum, A.; Ambre, A. H.; Katti, K. S.; Gange, K. N.; Srivastava, D. K.; Sarkar, K.; Mallik, S. Polymer Coated Echogenic Lipid Nanoparticles with Dual Release Triggers. *Biomacromolecules* **2013**, *14*, 841−853.
(52) Subik, K.; Lee, J. F.; Baxter, L.; Strzepek, T.; Costello, D.; Crowley, P.; Xing, L.; Hung, M. C.; Bonfiglio, T.; Hicks, D. G. The Expression Patterns of ER, PR, HER2, CK5/6, EGFR, Ki-67 and AR by Immunohistochemical Analysis in Breast Cancer Cell Lines. *Breast Cancer* **2010**, *4*, 35−41.
(53) Bhattacharya, D.; Das, M.; Mishra, D.; Banerjee, I.; Sahu, S. K.; Maiti, T. K.; Pramanik, P. Folate Receptor Targeted, Carboxymethyl Chitosan Functionalized Iron Oxide Nanoparticles: A Novel Ultradispersed Nanoconjugates for Bimodal Imaging. *Nanoscale* **2011**, *3*, 1653−1662.
(54) Hingorani, R.; Deng, J.; Elia, J.; McIntyre, C.; Mittar, D. Detection of Apoptosis Using the BD Annexin V FITC Assay on the BD FACSVerse System. https://www.bdbiosciences.com/documents/BD_FACSVerse_Apoptosis_Detection_AppNote.pdf (accessed Feb 2014).
(55) Ozaslan, M.; Karagoz, I. D.; Kilic, I. H.; Guldur, M. E. Ehrlich Ascites Carcinoma. *Afr. J. Biotechnol.* **2013**, *10*, 2375−2378.

DOI: 10.1021/acsami.5b01731
ACS Appl. Mater. Interfaces 2015, 7, 9211−9227

(56) Lale, S. V.; Kumar, A.; Naz, F.; Bharti, A. C.; Koul, V. Multifunctional ATRP based pH Responsive Polymeric Nanoparticles for Improved Doxorubicin Chemotherapy in Breast Cancer by Proton Sponge Effect/Endo-Lysosomal Escape. *Polym. Chem.* **2015**, *6*, 2115−2132.
(57) Elexpuru, A.; Soriano, M.; Villalobo, A. Characterization of the Epidermal Growth Factor Receptor from Ehrlich Ascites Tumor Cells. *Biol. Chem. Hoppe-Seyler* **1994**, *375*, 293−293.
(58) Soares, D. C. F.; de Oliveira, M. C.; de Barros, A. L. B.; Cardoso, V. N.; Ramaldes, G. A. Liposomes Radiolabeled with Gd, in Vitro Antitumoral Activity, Biodistribution Study and Scintigraphic Image in Ehrlich Tumor Bearing Mice. *Eur. J. Pharm. Sci.* **2011**, *43*, 290−296.
(59) Robinson, D. J.; Christenson, R. H. Creatine Kinase and its CK-MB Isoenzyme: The Conventional Marker for the Diagnosis of Acute Myocardial Infarction. *J. Emerg. Med.* **1999**, *17*, 95−104.

DOI: 10.1021/acsami.5b01731
ACS Appl. Mater. Interfaces 2015, 7, 9211−9227